Astronomy & Astrophysics

New mercury-manganese stars and candidates from LAMOST DR4

E. Paunzen[1], S. Hümmerich[2,3], and K. Bernhard[2,3]

[1] Department of Theoretical Physics and Astrophysics, Masaryk University, Kotlářská 2, 611 37 Brno, Czech Republic
e-mail: epaunzen@physics.muni.cz
[2] Bundesdeutsche Arbeitsgemeinschaft für Veränderliche Sterne e.V. (BAV), 12169 Berlin, Germany
[3] American Association of Variable Star Observers (AAVSO), 49 Bay State Rd, Cambridge, MA 02138, USA

ABSTRACT

Aims. The present work presents our efforts at identifying new mercury-manganese (HgMn/CP3) stars using spectra obtained with the Large Sky Area Multi-Object Fiber Spectroscopic Telescope (LAMOST).
Methods. Suitable candidates were searched for among pre-selected early-type spectra from LAMOST DR4 using a modified version of the MKCLASS code that probes several Hg II and Mn II features. The spectra of the resulting 332 candidates were visually inspected. Using parallax data and photometry from *Gaia* DR2, we investigated magnitudes, distances from the Sun, and the evolutionary status of our sample stars. We also searched for variable stars using diverse photometric survey sources.
Results. We present 99 bona fide CP3 stars, 19 good CP3 star candidates, and seven candidates. Our sample consists of mostly new discoveries and contains, on average, the faintest CP3 stars known (peak distribution $9.5 \leq G \leq 13.5$ mag). All stars are contained within the narrow spectral temperature-type range from B6 to B9.5, in excellent agreement with the expectations and the derived mass estimates ($2.4 \leq M_\odot \leq 4$ for most objects). Our sample stars are between 100 Myr and 500 Myr old and cover the whole age range from zero-age to terminal-age main sequence. They are almost homogeneously distributed at fractional ages on the main sequence $\leq 80\%$, with an apparent accumulation of objects between fractional ages of 50% to 80%. We find a significant impact of binarity on the mass and age estimates. Eight photometric variables were discovered, most of which show monoperiodic variability in agreement with rotational modulation.
Conclusions. Together with the recently published catalogue of APOGEE CP3 stars, our work significantly increases the sample size of known Galactic CP3 stars, paving the way for future in-depth statistical studies.

Key words. stars: chemically peculiar – stars: abundances – stars: variables: general

1. Introduction

A significant fraction of early B- to early F-type main-sequence stars exhibits peculiar atmospheric compositions that indicate abundance stratification due to atomic diffusion in their outer layers (e.g. Michaud 1970; Richer et al. 2000). These objects, which are generally referred to as chemically peculiar (CP) stars, have been divided into several groups according to their peculiarities. The four main groups are the CP1 stars (the metallic-line or Am/Fm stars), the CP2 stars (the magnetic Bp/Ap stars), the CP3 stars (the mercury-manganese or HgMn stars), and the CP4 stars (the He-weak stars) (Preston 1974). Further groups have been defined, such as the λ Bootis stars, which show peculiarly low surface abundances of iron-peak elements (Murphy & Paunzen 2017). In general, concerning the strength of the chemical peculiarities, there is a continuous transition from normal to peculiar stars (Loden & Sundman 1987).

Significant progress has been made in the understanding of the atomic diffusion process, for example concerning its interplay with parameters such as magnetic field strength and mass loss (Alecian & Stift 2017, 2019). Nevertheless, further refinement is necessary before the models will be able to reproduce the observed complex abundance patterns of CP stars in detail.

On average, CP3 stars rotate considerably slower than chemically normal main-sequence stars of similar temperatures

(Mathys 2004). They are encountered in the temperature range of $10\,500\,\mathrm{K} \leq T_{\mathrm{eff}} \leq 16\,000\,\mathrm{K}$ and mainly characterised by the presence of strong atmospheric overabundances of Hg and Mn as compared to the solar values (up to 6 and 3 dex, respectively; Smith 1996; Ghazaryan & Alecian 2016). However, their spectra show numerous other peculiarities and often indicate strikingly different abundance patterns from one star to another. As a general rule, heavy elements are overabundant, with the strength of the overabundances increasing with atomic number (Castelli & Hubrig 2004; Ghazaryan & Alecian 2016). A good summary of the observed peculiarities in CP3 stars is provided by Ghazaryan & Alecian (2016).

Several studies indicated a multiplicity incidence of more than 50% among CP3 stars (Smith 1996). Hubrig & Mathys (1995) and Schöller et al. (2010), for instance, estimated that values may be as high as 67% and 91%, respectively. The tidal interaction induced by the presence of a companion star is thought to significantly impact the observed chemical peculiarities.

An inhomogeneous surface element distribution with obvious signs of secular evolution was identified in several CP3 stars (e.g. Hubrig & Mathys 1995; Adelman et al. 2002; Hubrig et al. 2006; Kochukhov et al. 2007; Briquet et al. 2010; Korhonen et al. 2013). Several mechanisms were proposed to explain the observed abundance inhomogeneities, such as time-dependent atomic diffusion (Alecian et al. 2009) and atomic

diffusion in the presence of a weak, multi-polar magnetic field (Alecian 2012, 2013). CP3 stars have traditionally been grouped with the non-magnetic CP stars. While they certainly lack the strong organised magnetic fields of the CP2 and CP4 stars (the so-called magnetic CP stars or mCP stars), several studies indicated the presence of weak or tangled fields (Hubrig et al. 2010, 2012). These claims were disputed by other investigations (see the discussion and references in Kochukhov et al. 2013), and this remains a controversial issue. Recent evidence for the detection of variable, weak, and tangled magnetic fields in CP3 stars was presented by Hubrig et al. (2020).

Although theoretical modelling predicted the occurrence of pulsational instability via the κ mechanism (Turcotte & Richard 2003; Alecian et al. 2009) and CP3 stars share their position in the Hertzsprung-Russell (HR) diagram with pulsating variables such as the slowly pulsating B (SPB) stars, they are among the least photometrically variable CP stars (Adelman 1998), which suggests that important parameters are missing from the pulsation models. Since the advent of high-precision space photometry, however, an increasing number of photometrically variable CP3 stars has been identified. Still, no consensus has yet been reached as to the cause of the observed photometric variations, and arguments have been put forth in favour of both rotational as well as pulsational variability, with the more recent studies favouring rotational modulation due to abundance spots (cf. e.g. the discussion and references in Hümmerich et al. 2018).

Recently, Chojnowski et al. (2020) reported their efforts at identifying CP3 stars using SDSS/APOGEE H-band spectra. The authors identified suitable targets via the presence of Mn II and Ce III lines and presented a catalogue of 260 newly identified objects, thereby more than doubling the sample size of known Galactic CP3 stars (from ~194 to ~454 known objects; cf. Chojnowski et al. 2020).

Here we present our efforts at identifying new CP3 stars using archival spectra from the fourth data release (DR4) of the Large Sky Area Multi-Object Fiber Spectroscopic Telescope (LAMOST) of the Chinese Academy of Science (Zhao et al. 2012; Cui et al. 2012). We have identified 99 bona fide CP3 stars, 19 very good CP3 star candidates, and seven candidates. Most of these stars are new discoveries; only 15 stars of our sample are contained in the catalogue of Chojnowski et al. (2020). Thus, including the very good candidates, we further increase the number of known CP3 stars to more than 550 objects. Furthermore, with a broad peak distribution between G magnitudes 9.5 and 13.5, our sample contains on average the faintest CP3 stars known.

Together with the work of Chojnowski et al. (2020), our study significantly increases the sample size of known Galactic CP3 stars, which will benefit future in-depth statistical studies and theoretical modelling attempts alike. Section 2 discusses spectroscopic data and sample selection process and details the spectral classification workflow. Section 3 provides a discussion of our results, such as spectral classifications, evolutionary status, and photometric variability of our sample stars. We conclude in Sect. 4.

2. Spectroscopic data and sample selection

This section provides descriptions of the LAMOST spectral archive, the MKCLASS spectral classification code, the sample selection process, and the spectral classification workflow.

2.1. The Large Sky Area Multi-Object Fiber Spectroscopic Telescope (LAMOST)

The LAMOST telescope[1] (Zhao et al. 2012; Cui et al. 2012) is located at the Xinglong Observatory in Beijing, China. It is a Schmidt telescope with an effective aperture of 3.6−4.9 m (field of view of about 5°), which was designed to collect 4000 spectra in a single exposure (spectral resolution $R \sim 1800$, limiting magnitude $r \sim 19$ mag, wavelength coverage 3700 to 9000 Å). The LAMOST telescope is therefore well suited to carry out large-scale spectral surveys and is currently executing a survey of the entire available northern sky. LAMOST spectra are made available to the public in consecutive data releases via the LAMOST spectral archive[2]. Alreading containing a total of 14.48 million spectra as of DR7 (31 March 2020), the LAMOST archive is a prime resource for researchers, whose exploitation has only just begun.

Several investigations used LAMOST spectra to study CP stars. For instance, Hou et al. (2015) and Qin et al. (2019) searched for CP1 stars in the low-resolution spectra of DR1 and DR5, respectively. Our efforts in the identification and classification of mCP stars using spectra from DR4 led to the identification of a sample of 1002 mCP stars, comprising mostly new discoveries (Hümmerich et al. 2020).

2.2. Sample selection process

As a first step, we cross-matched the complete LAMOST DR4 archive with the Gaia DR2 catalogue (Gaia Collaboration 2016, 2018; Arenou et al. 2018) and utilised the G versus ($BP-RP$) diagram to impose a cut on the investigated spectral type range, selecting only stars with ($BP-RP$) < 0.45 mag (i.e. hotter than spectral type mid F). The limit was extended down to this colour range in order not to exclude reddened early-type stars. Because this colour-based approach will still miss highly reddened early-type objects, such as stars in the Galactic disk, or objects with bad Gaia photometry, additional B- and A-type stars were selected via the spectral types listed in the DR4 VizieR online catalogue (Luo et al. 2018)[3]. From the resulting list of stars, we excluded apparent supergiants and objects having spectra with a S/N of less than 50 in the Sloan g band. About 45 000 spectra were discarded in this manner. This cut was imposed because the detection of CP star features in objects with $S/N < 50$ is difficult (Paunzen et al. 2011). In the case of objects having more than one spectrum in the DR4 catalogue, we considered only the spectrum with the highest Sloan g band S/N.

In a second step, all remaining spectra were classified with the MKCLASS_HgMn code using all four libraries (*libr18*, *libnor36*, *libsynth*, *liblamost*). To identify CP3 star candidates, we counted the number of detections $N_{det}(\lambda)$ of a peculiarly strong Hg II and Mn II feature at or around the specified wavelength (Å) with the different standard star libraries (cf. Table 2). The resulting value ($0 \leq N_{det}(\lambda) \leq 4$) provides an estimation of significance: $N_{det}(\lambda) = 4$ was considered to be a robust detection, while $N_{det}(\lambda) < 2$ detections were viewed with caution. For convenience, the number of detections of the different Mn II features were added up to yield $N_{det}(Mn\_all)$. A sample output of MKCLASS_HgMn is provided in column two of Table 3.
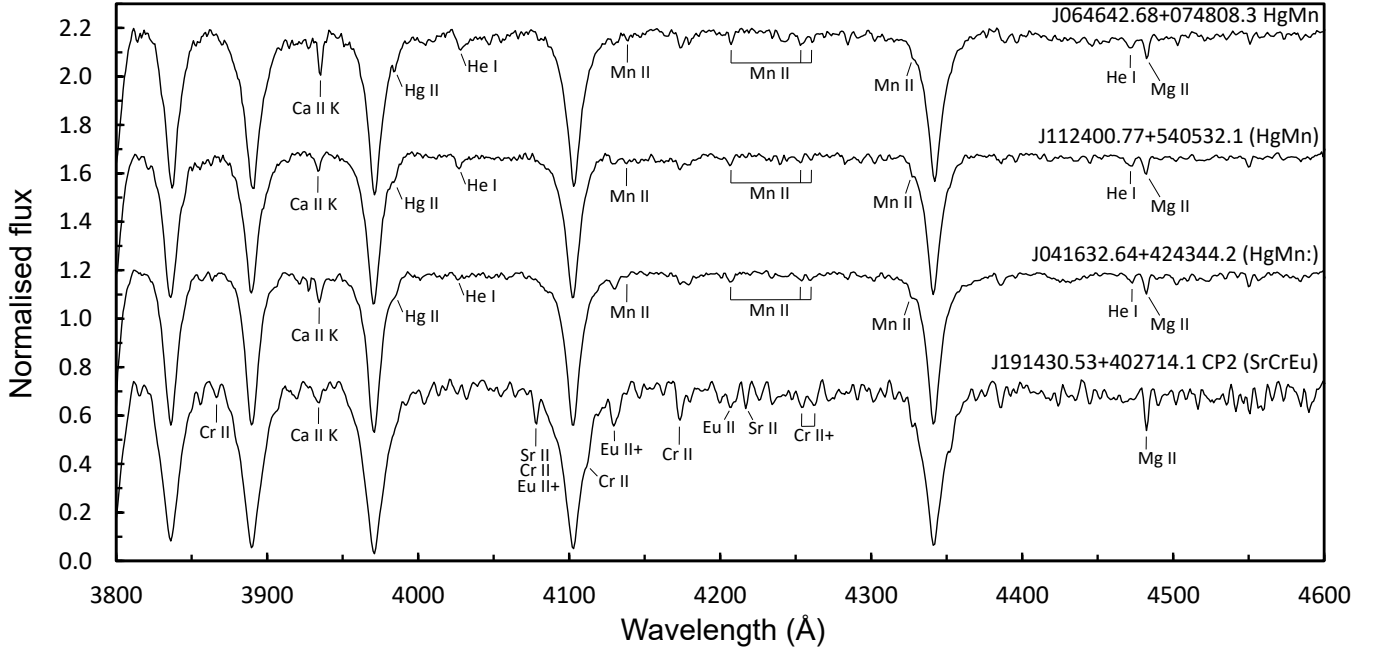

Fig. 1. Blue-violet region of the LAMOST DR4 spectra of (from top to bottom) the bona fide CP3 star LAMOST J064642.68+074808.3, the good CP3 star candidate LAMOST J112400.77+540532.1, the CP3 star candidate LAMOST J041632.64+424344.2, and the CP2 star LAMOST J191430.53+402714.1. Some prominent lines of interest are identified.

All stars satisfying the criteria $N_{\text{det}}(\lambda 3984) > 0$ and $N_{\text{det}}(\text{Mn\_all}) > 0$ were assigned candidate status, which resulted in a candidate sample of 332 stars. As next step, the spectra of all these objects were visually inspected to sort out bona fide CP3 stars and CP3 star candidates. To this end, the spectra were overlaid with and compared to the spectrum of α and as shown in Fig. 4.16 of Gray & Corbally (2009) and the strength of the Hg II and Mn II features was assessed. Depending on a visual estimate of the strength and clarity of the CP3 star features in the spectrum, stars were classified as either (i) bona fide CP3 stars, (ii) good CP3 star candidates, or (iii) CP3 star candidates. Figure 1 illustrates this process by showing the spectra of the bona fide (group i) CP3 star LAMOST J064642.68+074808.3, the good CP3 star candidate (group ii) LAMOST J112400.77+540532.1, and the CP3 star candidate (group iii) LAMOST J041632.64+424344.2. The CP3 status of stars of groups (ii) and (iii) should be confirmed by additional high-resolution spectroscopic observations.

Roughly a third of the investigated stars ($N = 125$) turned out to be either bona fide CP3 stars or candidates, which highlights that the chosen approach is a viable way of identifying CP3 stars in massive spectral archives. The other two thirds are made up of stars with spectra of very low S/N (which we discarded), spectra showing artefacts at the position of the probed wavelengths (in particular null flux at 3984 Å), several apparently chemically normal stars, a handful of Be stars, and about 60 CP2 stars. The high number of CP2 stars is not surprising, as these objects may also show overabundances of Mn, or, more often, other strong features at the probed wavelengths. This is illustrated in the bottom panel of Fig. 1, which shows the spectrum of the known CP2 star LAMOST J191430.53+402714.1 (spectral type B9 IV–V CrEu; Hümmerich et al. 2020) that was recovered with the MKCLASS_HgMn code. The strong Eu II 4205 Å line, in particular, can be confused with Mn II 4206 Å. This actually happened with a significant number of stars for which both a strong Eu II 4205 Å and a Mn II 4206 Å lines were identified

by the code (cf. Table 3). This confusing redundancy in output will be addressed by a future update of the code. Furthermore, strong metal lines in the spectral region from 4248 Å to 4262 Å may be misidentified as Mn II 4252/9 Å. In the case of LAMOST J191430.53+402714.1 (Fig. 1), we find strong absorption features centred on 4254 Å and 4262 Å. We assume that these are mostly caused by strong Cr I 4254.331 Å, Cr II 4254.56 Å, and Cr II 4261.92 Å lines, which goes along well with the observed significant overabundance of Cr as judged from the corresponding strong lines at 3866 Å, 4111 Å, and 4172 Å.

2.3. The MKCLASS code

2.3.1. General overview

The MKCLASS code was written by Richard O. Gray to classify stellar spectra on the Morgan-Keenan-Kellman (MKK) system in a way similar to a human classifier (Gray & Corbally 2014). In its current version (v1.07), MKCLASS works with spectra in the violet-green region (3800−5600 Å) in either rectified or flux-calibrated format. Several studies employed MKCLASS for the classification of a multitude of stellar spectra (e.g. Gray & Corbally 2014; Gray et al. 2016; Hümmerich et al. 2018, 2020) and demonstrated that its results compare favourably to manually derived classifications if input spectra of sufficient signal-to-noise (S/N) are provided. Typical temperature class and luminosity class uncertainties are of the order of 0.6 and 0.5 subclass, respectively (Gray & Corbally 2014).

As a first step, MKCLASS assigns a rough spectral type, which is subsequently refined by direct comparison with spectra from MKK standard star libraries. Two libraries of standard spectra are recommended for use with MKCLASS, which were obtained with the Gray/Miller spectrograph on the 0.8 m reflector of the Dark Sky Observatory (North Carolina, USA): the *libr18* library, which consists of rectified spectra in the

Table 1. Characteristics of the spectral libraries used as standard star libraries for the modified version of the MKCLASS code in the present study.

Library	Characteristics
libr18	Spectral range from 3800−4600 Å, resolution of 1.8 Å ($R \sim 2200$), normalised and rectified spectra; all luminosity classes (Ia–V)
libnor36	Spectral range from 3800−5600 Å, resolution of 3.6 Å ($R \sim 1100$), flux-calibrated and normalised spectra; all luminosity classes (Ia–V)
libsynth	Spectral range from 3800−4600 Å, smoothed to a resolution of 3.0 Å and an output spacing of 0.5 Å, flux-calibrated and normalised synthetic spectra; only dwarf spectra (luminosity class V); spectral types B5 to F5
liblamost	Spectral range from 3800−5600 Å, resolution $R \sim 1800$, flux-calibrated and normalised spectra; only dwarf and giant spectra (luminosity classes V and III); spectral types B3 to G0

spectral range 3800−4600 Å (resolution of 1.8 Å), and the *libnor36* library, which encompasses flux-calibrated and normalised spectra in the spectral range from 3800−5600 Å (resolution of 3.6 Å). However, it is also possible to employ additional spectral libraries specifically tailored to the needs of the researcher.

In its current implementation, MKCLASS is capable of identifying a set of spectral peculiarities that are relevant to the classification of objects such as CP1 and CP2 stars, barium stars, or carbon-rich giants. Unfortunately, the original code does not probe any lines relevant to the identification of CP3 stars. For more information on the MKCLASS code and its usage, we refer the reader to Gray & Corbally (2014) and the corresponding website[4].

2.3.2. Customising the MKCLASS code

Our previous LAMOST-based study (Hümmerich et al. 2020) was concerned with the identification and classification of mCP stars using low-resolution spectra from DR4. To this end, we produced a modified version of the MKCLASS code (termed MKCLASS_mCP) capable of probing a number of spectral features related to Si, Cr, Sr, Eu, and He abundances, which are helpful in the identification and classification of these objects (cf. Table 2). Furthermore, in addition to using the *libr18* and *libnor36* libraries that come with MKCLASS, two further standard star libraries were employed: the *libsynth* library, which contains spectra synthesised with the SPEC-TRUM code[5] (Gray & Corbally 1994) and ATLAS9 model atmospheres (Castelli et al. 2003), and the *liblamost* library, which consists of a grid of suitable high S/N LAMOST DR4 spectra chosen from the list of Gray et al. (2016). The characteristics of the different libraries, which have also been employed in the present study, are summarised in Table 1. For more information on the MKCLASS_mCP code and the *libsynth* and *liblamost* libraries, the reader is referred to Hümmerich et al. (2020).

In our search for mCP stars, suitable candidates were chosen from a colour-selected sample of early-type objects via the presence of the conspicuous 5200 Å flux depression, which is a characteristic of this subgroup of CP stars and relatively easy to identify even at the low resolution of the employed LAMOST spectra (Hümmerich et al. 2020). Unfortunately, no similarly convenient spectral feature is available for the identification of CP3 stars. Therefore, we altered the MKCLASS_mCP code to additionally probe suitable Hg II and Mn II lines and blends in

Table 2. Absorption lines and blends identified by the modified versions of the MKCLASS code.

(1) Blend/Line	(2) Wavelength (Å)	(3) SpT_range
(Si II/Cr II/Sr II)	4076/77	B7−F5
(Si II/Eu II)	4128/30	B3−F2
Si II	3856	B3−F2
Si II	4200	B3−A2
Si II	5041	B3−F2
Si II	5056	B3−F2
Si II	6347	B3−F2
Si II	6371	B3−F2
Cr II	3866	B7−F2
Cr II	4172	B7−F2
Sr II	4216	B7−F2
Eu II	4205	B7−F2
He I	4009	B0−A0
He I	4026	B0−A0
He I	4144	B0−A0
He I	4387	B0−A0
Hg II	**3984**	**O6−A3**
Mn II	**4136**	**O6−A3**
Mn II	**4206**	**O6−A3**
Mn II	**4252/9** [a]	**O6−A3**

Notes. Normal font denotes features identified by the MKCLASS_mCP code (Hümmerich et al. 2020), bold font the additional lines used for the identification of CP3 stars by the MKCLASS_HgMn code. The columns denote: (1) Blend/Line. (2) Wavelength (Å). (3) Spectral range in which the corresponding feature was probed. At the resolution of the LAMOST low-resolution spectra, all features listed in Table 2 are, to some extent, blended with other absorption lines. Nevertheless, the specified elements generally constitute the main contributors to these blends in the investigated groups of CP stars. [a]Although these lines are partly resolved in low- resolution LAMOST spectra, we chose to probe the blend of the region from 4248 to 4262 Å.

the blue-violet spectral region, which are relevant to the identification of CP3 stars. The choice of lines was influenced by the resolution of the LAMOST spectra and the availability of neighbouring continuum windows to probe a certain feature. After some experimentation, we came up with the lines and blends presented in Table 2 (bold font) as best choice. Although the Mn II 4252 Å and Mn II 4259 Å lines are partly resolved in LAMOST spectra, we chose to probe the blend of the region from 4248 Å

---

[4] http://www.appstate.edu/~grayro/mkclass/
[5] https://www.appstate.edu/~grayro/spectrum/spectrum.html

Table 3. Spectral classifications derived by the MKCLASS_HgMn code.

(1)	(2)	(3)	(4)	(5)	(6)	(7)	(8)
LAMOST_ID	Output using *libr18/libnor36/libsynth/liblamost*	$N_{\mathrm{det}}(\lambda3984)$	$N_{\mathrm{det}}(\lambda4136)$	$N_{\mathrm{det}}(\lambda4206)$	$N_{\mathrm{det}}(\lambda4252/9)$	$N_{\mathrm{det}}(\mathrm{Mn\_all})$	SpT_final
J000118.65+464355.0	A0 II−III Eu4205 Hg3984 Mn4259 ? B9 III Eu4205 B9.5 III	1	0	0	1	1	B9.5 III HgMn
J002635.94+562206.5	A0 II−III Eu4205 Hg3984 Mn4136 Mn4206 B8 V Eu4205 Mn4206 B8 IV Eu4205 Hg3984 Mn4136 B9 IV−V	2	2	2	0	4	B9 IV-V HgMn
J020922.72+533908.6	B7 V Eu4205 Mn4136 Mn4206 B8 IV Eu4205 Hg3984 Mn4136 Mn4206 B8 IV Eu4205 Hg3984 Mn4136 Mn4206 B9 III−IV	2	3	3	0	6	B8 IV HgMn
J030852.02+553734.3	B8 III−IV Eu4205 Hg3984 Mn4206 Mn4259 B7 III−IV Eu4205 Hg3984 Mn4206 Mn4259 B8 III Eu4205 Hg3984 Mn4206 Mn4259 B0 0 Mn4206 Mn4259	3	0	4	4	8	B8 IV HgMn
J031312.82+493559.8	A0 II−III Eu4205 Hg3984 Mn4136 ? B9 III Eu4205 B9 III−IV	1	1	0	0	1	B9 III-IV HgMn
J031943.49+561329.7	B7 III Eu4205 Mn4206 B5 III Hg3984 Mn4206 B7 III Eu4205 Mn4206 ?	1	0	3	0	3	B7 III HgMn
J032252.69+582806.7	B6 IV Mn4136 Mn4206 Mn4259 B7 III−IV Mn4206 Mn4259 B8 III−IV Eu4205 Mn4206 Mn4259 B6 IV Mn4136 Mn4206 Mn4259	0	2	4	4	10	B6 IV HgMn
J033700.61+571139.0	A0 II−III bl4077 Eu4205 Hg3984 B9 III−IV bl4077 Eu4205 B9 IV bl4077 Eu4205 B9 IV bl4077	1	0	0	0	0	B9 IV (HgMn)
J033939.69+473758.3	A0 II Eu4205 Mn4136 Mn4206 B8 IV Eu4205 Hg3984 Mn4136 Mn4206 B9 II−III Eu4205 B8 IV Hg3984 Mn4136 Mn4206	2	3	3	0	6	B8 IV HgMn
J034903.76+454037.3	B9 III−IV Eu4205 Hg3984 Mn4259 B9 IV Eu4205 B9 IV Eu4205 B9 IV−V	1	0	0	1	1	B9 IV HgMn

Notes. The columns denote: (1) LAMOST identifier. (2) "raw" MKCLASS_HgMn output using the standard star libraries *libr18*, *libnor36*, *libsynth*, and *liblamost*. (3)−(6) Number of detections N_{det} of a peculiarly strong line at the specified wavelength (Å) using all four libraries. (7) Number of detections across all investigated Mn II lines. (8) MKCLASS final type.

to 4262 Å, which yielded more promising results. These features were searched for in the spectral type range from O6 to A3, in addition to the other lines and blends listed in Table 2.

We note that at the resolution of the LAMOST low-resolution spectra, all features listed in Table 2 are, to some extent, blended with other absorption lines. Nevertheless, the specified elements generally constitute the main contributors to these blends in the investigated groups of CP stars. For example, the 3984 Å feature, which is particularly relevant to the identification of CP3 stars, is a complex blend, which, apart from the Hg II line, may include contributions from Cr I 3983.896 Å, Mn I 3983.683 Å, Fe I 3983.835 Å, and Fe I 3983.959 Å. However, the listed lines mostly play a part in the cooler CP2 stars (Preston 1973). In the temperature regime of the CP3 stars, the density of lines is rather low and we generally do not expect significant blending of the Hg II 3984 Å line (Cowley & Aikman 1975). This is confirmed by data from the Vienna Atomic Line Database (VALD; Kupka et al. 1999), which indicate no other strong lines in the corresponding wavelength region for the investigated effective temperature range.

Nevertheless, at LAMOST resolution, the 3984 Å feature also contains contributions from the Y II line at 3982.59 Å. Y is strongly overabundant in CP stars (Guthrie 1971; Monier et al. 2019), in particularly in CP3 stars. From the compilation of Ghazaryan et al. (2018), we derive mean Y abundances of +0.86 dex, +1.26 dex, and +2.64 dex as compared to the solar value for, respectively, CP1, CP2, and CP3 stars. However, considering the strength of the Y II spectrum, at the resolution of the LAMOST spectra, an extreme overabundance of Y would be needed for a significant detection of the Y II 3982.59 Å line alone. Monier et al. (2020), for example, illustrate the spectrum of the CP3 star HR 8937, which shows an Y overabundance of +4 dex. Line depths in this spectrum reach 12% for the Y II line, which should be retraceable from LAMOST spectra, and 25% for the neighbouring Hg II line. At low resolution, the corresponding blend of both lines would therefore be clearly dominated by the Hg II line.

In summary, while contributions from the Y II 3982.59 Å line are expected, we are confident that the Hg II 3894 Å line is the main contributor to the 3984 Å blend observed in our
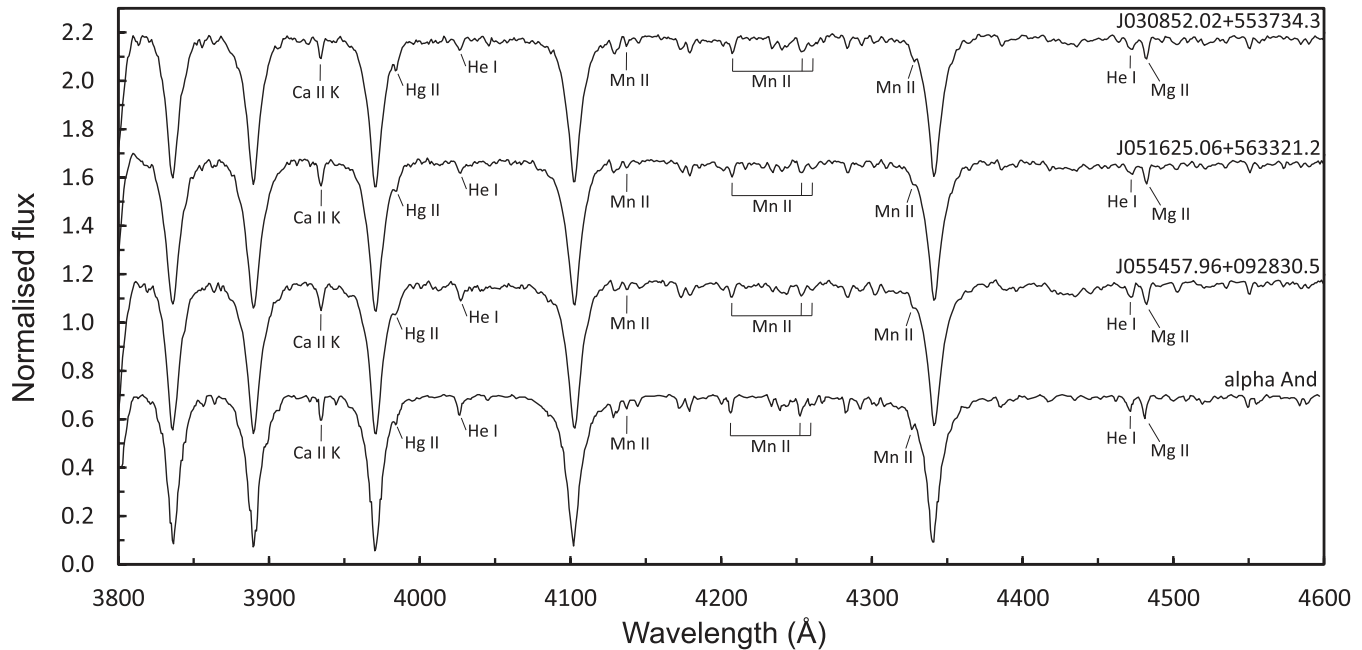
Fig. 2. Showcase of three newly identified bona fide CP3 stars, illustrating the blue-violet region of the LAMOST DR4 spectra of (from top to bottom) LAMOST J030852.02+553734.3 (B8 IV HgMn), LAMOST J051625.06+563321.2 (B7 IV–V HgMn), and LAMOST J055457.96+092830.5 (B8 IV HgMn). The bottom spectrum is that of α And as adapted from Fig. 4.16 of Gray & Corbally (2009). The spectral types in parentheses correspond to the MKCLASS final types. Some prominent lines of interest are identified.

sample stars. This is in line with the common practice to use the 3984 Å feature to identify CP3 stars in classification resolution spectra (e.g., Gray & Corbally 2009), in particular as the Hg II 3984 Å line is generally not prominent in the other groups of CP stars (Gray & Corbally 2009). For instance, none of the CP2 star LAMOST spectra investigated in Hümmerich et al. (2020) shows a feature of comparable strength in the 3984 Å region. Together with the obvious Mn II features observed in our sample stars, the strong 3984 Å blend seems to be a unique characteristic of the group of CP3 stars.

We stress that the altered version of the MKCLASS code, which was derived from the MKCLASS_mCP code and is referred to hereafter as MKCLASS_HgMn, was specifically created to work with LAMOST low-resolution spectra. Applying the code to spectra of other resolutions will require a corresponding update of the peculiarity classification routine and, perhaps, of the employed standard star libraries. We also caution against using the *libsynth* and *liblamost* libraries outside the context of this study, in particular as they do not contain stars of luminosity classes I and II (*liblamost*) and I, II, and III (*libsynth*).

3. Results

3.1. Spectral classification

For most stars, the spectral types derived with the four different spectral libraries are in good agreement. For the final classification, we followed the methodology of Hümmerich et al. (2020). In summary, whenever a spectral type was derived more than once across the different spectral libraries, the most common spectral type was adopted as the final classification. If no common classifications existed, spectral types were favoured in the order *liblamost > libsynth > libnor36 > libr18*. In the case of striking discrepancies, the corresponding spectra were visually inspected and the best-fitting type was adopted. For con-

venience, the final adopted classification is termed hereafter the "MKCLASS final type".

MKCLASS final types for all sample stars are presented in Table A.1. Bona fide CP3 stars, good CP3 star candidates, and CP3 star candidates can be identified by, respectively, the suffixes HgMn, (HgMn), and (HgMn:). Only three stars (LAMOST J052308.77+323128.3, LAMOST J055400.30+290112.2, and LAMOST J062503.02+033237.3) are common with the list of Renson & Manfroid (2009). However, none of these objects was classified as a CP3 star. They are identified and shortly commented on in Table A.1. Furthermore, stars contained in the sample of Chojnowski et al. (2020) are indicated by a corresponding footnote behind the LAMOST identifier in column two of this table. Figure 2 illustrates the spectra of three newly identified bona fide CP3 stars.

In accordance with the expectations for CP3 stars, all our sample stars are contained within the rather narrow spectral temperature-type range from B6 to B9.5 (Fig. 3). This is in excellent agreement with the derived mass estimates (cf. Sect. 3.3.2), which we interpret as independent proof of the applicability of our approach and the validity of the spectral classifications.

3.2. Magnitudes, distances from the Sun, and cluster membership

Histograms of the G magnitudes and distances from the Sun are shown in Figs. 4 and 5. The magnitude distribution of our sample stars has a broad maximum between G magnitudes 9.5 and 13.5. Our sample stars, therefore, are on average significantly fainter than the CP3 stars listed in the catalogues of Renson & Manfroid (2009) and Chojnowski et al. (2020) (cf. Fig. 4). Most of our sample stars have distances between 500 pc and 2.5 kpc. There are only five objects within 500 pc from the Sun and nine objects with distances exceeding 2.5 kpc. In summary, our sample is a perfect extension to the CP3 stars listed in the above mentioned catalogues.
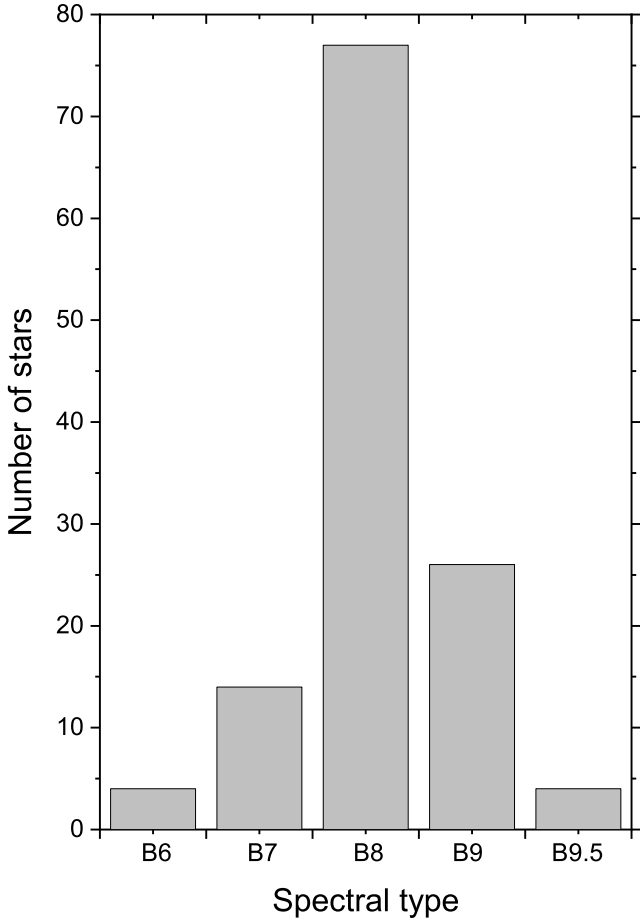
Fig. 3. Histogram of the spectral temperature-type distribution of our sample stars.

Fig. 4. Histograms of the G magnitudes for the CP3 stars from Renson & Manfroid (2009) (black dashed line), Chojnowski et al. (2020) (blue dotted line), and our sample (red solid line).

Several CP3 stars are known to be members of open clusters (e.g. Hubrig et al. 2012), which allows a reliable age determination. LAMOST generally avoids dense regions of the sky such as star clusters. Nevertheless, we searched for possible cluster members among our sample stars within 3σ of the positions, diameter, proper motions, distances and their errors of star clusters from Kharchenko et al. (2013) and Cantat-Gaudin et al. (2018). Only one match was found: According to our data, LAMOST J041533.86+493944.1 belongs to the open cluster NGC 1528, an intermediate age (about 350 Myr old) open cluster (Kharchenko et al. 2013) with no known CP stars. The evolutionary status of this star is further investigated in Sect. 3.3.2.

3.3. Evolutionary status

Here we consider the evolutionary status of our sample stars, discuss their properties in the $(BP-RP)_0$ versus $M_{G,0}$ and mass versus fractional age on the main-sequence spaces, and investigate the influences of binarity and overall metallicity on our results.

3.3.1. Colour-magnitude diagram

The colour-magnitude diagram (CMD) was constructed using the homogeneous *Gaia* DR2 photometry from Arenou et al. (2018). As most of our sample stars are members of the Galactic disk and situated beyond 500 pc from the Sun, interstellar
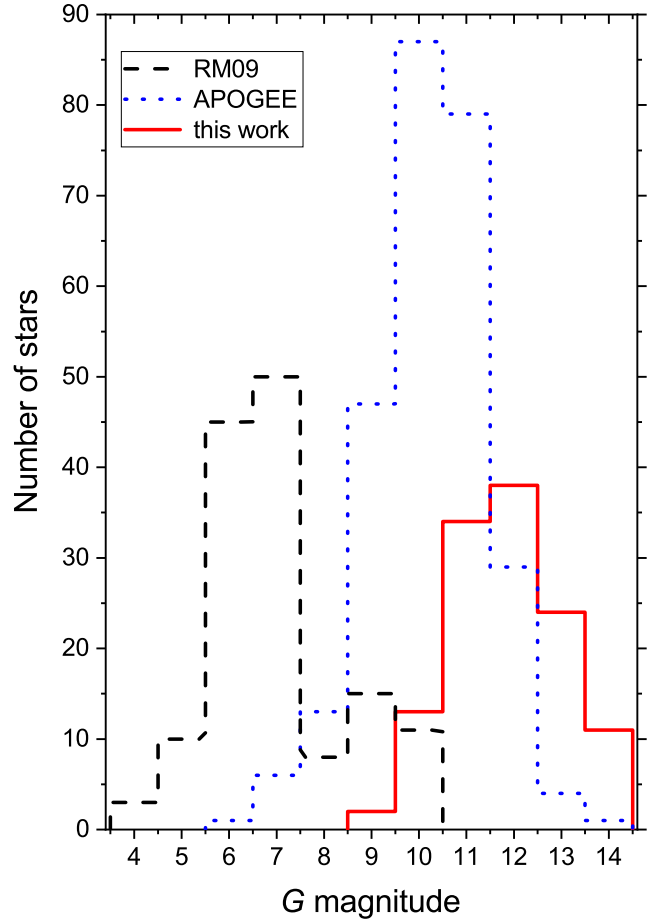
reddening (absorption) needs to be taken into account. Unfortunately, Strömgren-Crawford indices, which allow a reliable reddening estimation, are not available for most of our sample stars (Paunzen 2015). We therefore relied on the reddening map of Green et al. (2018) and directly converted parallaxes to distances in order to interpolate within this map. Reddening values were transformed using the relations

$$E(B-V) = 0.76E(BP-RP) = 0.40A_G, \qquad (1)$$

which take into account the coefficients listed in Green et al. (2018).

Figure 6 illustrates the CMD of our sample stars, the reddening vector according to an uncertainty of 0.1 mag for $E(B-V)$, and PARSEC isochrones (Bressan et al. 2012) for solar metallicity $[Z] = 0.02$ dex[6]. Considering the errors, eight stars are situated well below the zero-age main sequence (ZAMS). Their position cannot be explained by errors in the reddening estimation process and is likely due to inconsistent photometry. We are unable to shed more light on this matter with the available data.

The following three stars are characterised by their peculiar positions in the CMD and deserve further attention:

LAMOST J033700.61+571139.0 (B9 IV (HgMn)). The derived age of about 3 Gyr and the star's very red colour are

---

[6] We favour this value of solar metallicity because it has been shown to agree with recent results of helioseismology (Vagnozzi 2019).
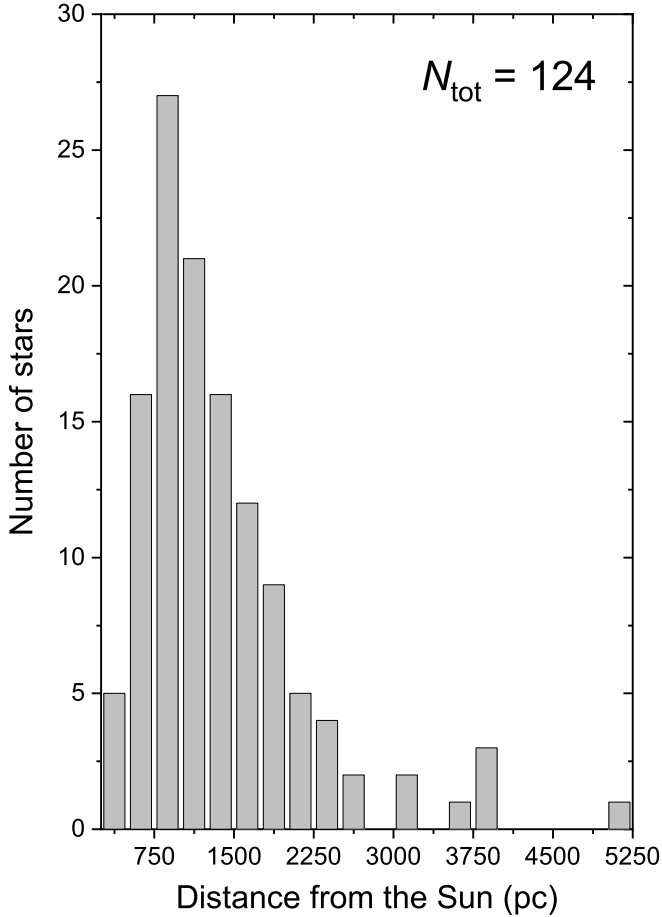
Fig. 5. Histogram of the distances from the Sun. Parallax measurements from the *Gaia* DR2 catalogue are available for all sample stars, with the single exception of LAMOST J031312.82+493559.8.

Fig. 6. $(BP-RP)_0$ versus $M_{G,0}$ diagram of our sample stars. Also indicated are PARSEC isochrones for solar metallicity $[Z] = 0.02$ dex. Ages are given in logarithmic units. The arrow indicates the reddening vector according to an uncertainty of 0.1 mag for $E(B-V)$. Red and blue symbols denote, respectively, bona fide CP3 stars and CP3 star candidates.

not compatible with the available spectrum that clearly indicates a late B-type star and was classified accordingly by the MKCLASS_HgMn code. The star is situated only about 260 pc from the Sun, which rules out strong and underestimated reddening as cause of the observed aberrant colours. However, the spectral energy distribution (SED) is best fit with an effective temperature of 6000 K. To exclude identification issues, we double checked the identifications of the LAMOST spectrum and the photometry employed for the SED fitting; no misidentifications were detected. In the literature, we also find widely different effective temperature estimates for this star: 5325 K (Ammons et al. 2006), 6210 K (Stassun et al. 2019), 6785 K (Bai et al. 2019), 7950 K (Xiang et al. 2019), and 9500 K (Bai et al. 2018). The wide range of different temperature values points towards a spectroscopic binary system observed at different phases. Further spectroscopic data are needed to shed more light on the nature of this peculiar object.

LAMOST J063246.02+030319.1 (B8 IV HgMn). The estimated visual absorption in the line-of-sight to this star amounts to $A_V = 2.42$ mag. A correction of about one magnitude would be necessary to shift its position to the ZAMS in the CMD. On close inspection, the reddening map of Green et al. (2018) reveals a significant source of absorption between 1.2 and 3.2 kpc, with LAMOST J063246.02+030319.1 being situated just on the edge of the most dense region of the extinction source. According to Bailer-Jones et al. (2018), the distance range for this star
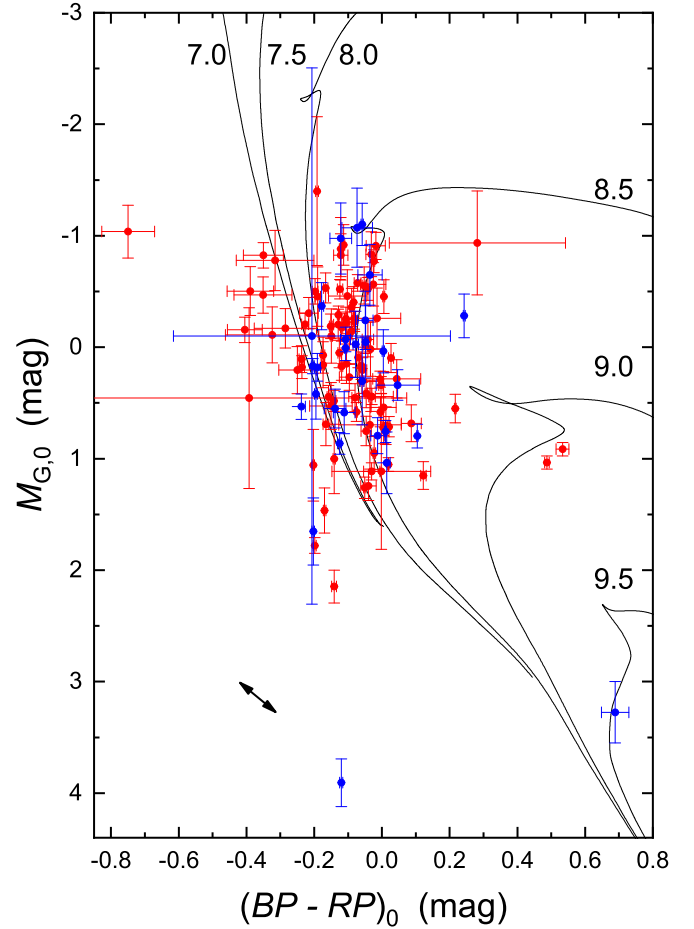
amounts to 1.2 to 1.4 kpc. A direct conversion of the parallax yields a distance of 1.36 kpc with an error of about 9%, in agreement with the aforementioned result. We therefore assume that the line-of-sight extinction is significantly smaller than suggested by the reddening map, which is supported by the absorption value of $A_G = 1.18$ mag listed in the *Gaia* DR2 catalogue.

LAMOST J112400.77+540532.1 (B8 IV (HgMn:)). This star appears about three magnitudes too faint for its colour. It also shows a very large proper motion [−25.539, −5.957 mas yr⁻¹] and is situated only about 350 pc from the Sun. No further literature studies on this object are available. The star's location in the CMD would qualify it as a hot subdwarf (Pelisoli et al. 2019; Geier 2020). These objects are considered to be core helium-burning stars located at the blueward extension of the Horizontal Branch, the so called Extreme or Extended Horizontal Branch (EHB). To end up on the EHB, stars have to lose almost their entire hydrogen envelopes during the red-giant phase, which is most likely accomplished via binary mass transfer (Heber 2016). Strongly peculiar hot subdwarfs are known (Naslim et al. 2011). LAMOST J112400.77+540532.1 shows several peculiarities, such as strong features at 4136 Å, 4206 Å and 4252/9 Å, which we interpret as being due to Mn II, but only a slight bump at 3984 Å. Consequently, the star was classified as a CP3 star candidate. We encourage a detailed abundance analysis using

high-resolution spectroscopy to shed more light on the nature of this object.

From the distribution of stars in Fig. 6, we deduce that the majority of our sample stars is between 100 Myr and 500 Myr old. Several stars are obviously situated at or close to the ZAMS. To further interpret these findings, we need to consider the influences of multiplicity and the choice of the overall metallicity [Z] for the isochrones. The latter parameter has a significant influence on the derived ages (e.g. Bagnulo et al. 2006; Hümmerich et al. 2020).

Schöller et al. (2010) announced that up to ~90% of all CP3 stars are actually part of binary systems. In classification resolution spectra, only the most extreme double-lined spectroscopic (SB2) systems can be detected. Therefore, we had to resort to other data to estimate the binarity rate among our sample stars.

As a first step, we investigated the *Gaia* DR2 astrometric solutions because it has been shown that a large error may indicate binarity (Zavada & Píška 2020). Furthermore, the *Gaia* DR2 catalogue includes a flag called "duplicated_source", which, if set to one, may indicate stellar multiplicity, but also observational, cross-matching, or processing problems. This flag has been set for 20 of our sample stars. We visually inspected the surroundings of these objects using the ALADIN sky atlas (Bonnarel et al. 2000; Boch & Fernique 2014) and found two stars (LAMOST J040155.24+514923.5 and LAMOST J062503.02+033237.3) with a comparably bright star in the close angular vicinity as well as four objects (LAMOST J050338.55+234349.5, LAMOST J053419.30+302407.7, LAMOST J060619.07+345118.1, and LAMOST J072016.47+141320.6) with much fainter neighbouring stars. As judged by this technique, the other fourteen stars have "clean" surroundings.

We next investigated the parameter "astrometric_gof_al" (gofAL), which denotes the goodness-of-fit statistic of the astrometric solution for the source in the along-scan direction. For the calculation of this parameter, the "Gaussianised chi-square" statistic has been used, which should approximately follow a normal distribution with zero mean value and unit standard deviation for good fits. Values exceeding +3 indicate a bad fit to the data (Gaia Collaboration 2018) and might indicate binarity. 113 sample stars show values exceeding this limit up to values of several hundreds. Interestingly, most of the objects with large gofAL values also have non-zero values for the parameters "astrometric_excess_noise" and "astrometric_excess_noise_sig", which we interpret as a consistent and strong indication of binarity. In summary, using the outlined approach, only 12 objects (or 8% of our sample) show no indication of binarity, which is fully in line with the binarity fraction estimate of Schöller et al. (2010). It is therefore imperative that the effects of binarity are taken into account when determining the masses and ages of our sample stars (and, for that matter, any other sample of CP3 stars).

The employed PARSEC isochrones use scaled abundances according to the abundance pattern of the Sun, that is, they were calculated assuming standard chemical composition. It is an open question if, or to what extent, this assumption can also be applied to the highly peculiar CP3 stars, which often show quite individualistic abundance patterns. If diffusion is accepted as the main mechanism behind the formation of the observed peculiar atmospheric compositions, in agreement with the current paradigm, we expect that the surface composition is not representative of the stellar interior, which should have an overall abundance close to solar. Furthermore, the current isochrone calculations assume a [Z] value for the whole star; no corresponding
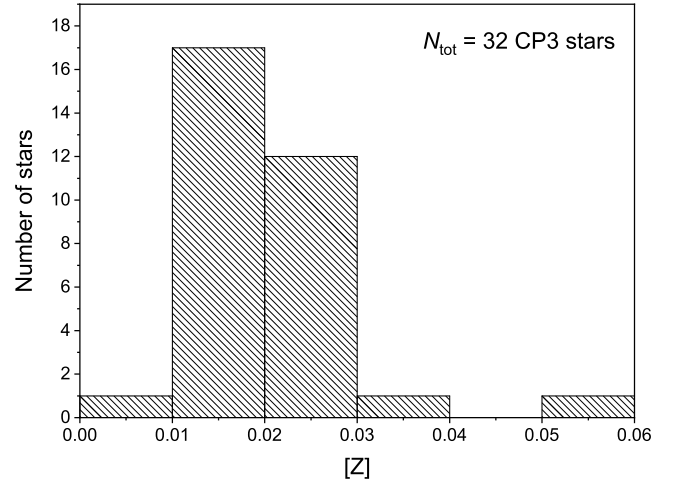

Fig. 7. Distribution of [Z] values for the CP3 stars from the Ghazaryan et al. (2018) catalogue with a least three measurements of C, N, O, and S. Almost all stars have an overall metallicity comparable to the solar value ([Z] = 0.02 dex).

calculations are available that can handle different [Z] values for different stellar layers.

To evaluate the effect of metallicity on the results, we examined the [Z] distribution for CP3 stars from the Ghazaryan et al. (2018) catalogue having at least three measurements of the light elements C, N, O, and S, which contribute the most to the derived [Z] values. In total, 32 CP3 stars fulfil this criterion. Figure 7 illustrates the distribution of the derived [Z] values. Unfortunately, no constraints on the corresponding errors could be estimated because the errors of the individual abundance determinations are mostly not available in the reference source. With the exception of only three stars, all objects show [Z] values between 0.01 and 0.03. Assuming a conservative error of about 10%, this is in agreement with the assumption of solar abundance [Z] = 0.02. Our choice of isochrones of solar abundance, therefore, seems justified and is not expected to introduce significant uncertainty.

3.3.2. Mass versus age on the main sequence

For theoretical considerations on the formation and evolution of CP3 stars, an accurate knowledge of their masses and ages is essential. It has already been emphasised that the majority of CP3 stars are contained within binary systems, a characteristic they share with the CP1 (Am/Fm) stars, with whom they may form a related sequence (cf. e.g. Smith 1974; Wahlgren & Dolk 1998). Questions like whether CP3 stars are homogeneously distributed over the main sequence are important to understand the role of angular momentum transfer between the companions and the diffusion time scale in their atmospheres.

In Fig. 8, we present the location of our sample stars in the $(BP-RP)_0$ versus $M_{G,0}$ diagram, with the exception of the three outliers discussed in Sect. 3.3.1. Also included are lines of constant masses and constant τ, which represents stellar age defined as the fraction of life spent on the main sequence, with the ZAMS corresponding to $\tau = 0\%$ and the terminal-age main sequence (TAMS) to $\tau = 100\%$. Again, we used PARSEC isochrones (Bressan et al. 2012) for solar metallicity [Z] = 0.02. We stress that these isochrones were calculated for single stars and can here only serve as an approximation.

Lines of constant τ are not evenly spaced in terms of $M_{G,0}$ and $(BP-RP)_0$. For instance, for a star with $3\,M_\odot$, the same $M_{G,0}$ interval of 0.45 mag is covered in the intervals from $0\% < \tau < 50\%$, $50\% < \tau < 80\%$, and $80\% < \tau < 100\%$. The difference in colour is unevenly spaced, too, with roughly the same intervals covered from $0\% < \tau < 80\%$ and $80\% < \tau < 100\%$. For lower mass stars, such as $2.4\,M_\odot$ objects, the colour difference from the ZAMS to the TAMS already amounts to 0.5 mag. As a consequence, depending on a star's location in the CMD, the size of the errors in both observables significantly impacts the final results.

As an overall conclusion from Fig. 8, most stars have masses between 2.4 and $4\,M_\odot$, which corresponds to spectral types between B9.5 V and B6 V. This is in excellent agreement with the derived spectral types; without a single exception, all sample stars are found in the specified range (cf. Fig. 3). Furthermore, our sample stars occupy the whole age range from ZAMS to TAMS, with an apparent accumulation of objects between $50\% < \tau < 80\%$.

To examine the effects of multiplicity on our results, knowledge of the mass ratio (q) of the components is necessary. In the literature (e.g. Ryabchikova 1998; Hubrig et al. 2012), mass ratios between 0.45 and 0.98 have been published for well investigated systems including at least one CP3 star component. We note that these results might be observationally biased as low-mass main-sequence companions are more difficult to detect using, for example, radial velocity studies.

In the following considerations, only binary systems, that is, systems with two components, were considered. For equal masses, the maximum expected effect amounts to 0.754 mag in terms of absolute magnitude, in the sense that the individual components are actually 0.754 mag fainter that an assumed companionless star in the $(BP-RP)_0$ versus $M_{G,0}$ diagram. However, as becomes obvious from Fig. 9, colour and absolute magnitude change depending on the mass of the primary, hence the situation is complex. The upper panel illustrates the grids for different q values, as calculated for primary masses of 4, 3, 2.5, and $2\,M_\odot$ using an isochrone for $\log t = 8.25$. The effect becomes noticeable in $M_{G,0}$ for $q > 0.5$ and reaches values of up to 0.1 mag in $(BP-RP)_0$. In consequence, without the knowledge of q, a correction for the effects of binarity is impossible to do on solid grounds.

The red curves in the lower panel of Fig. 9 show the situation for different masses and τ values. During the "horizontal phase" of the curves (up to $q < 0.6$ for $M = 2.5\,M_\odot$), the positions of the stars initially shift to higher τ values and then to lower ones. As mentioned before, lines of constant τ are not evenly distributed in the $M_{G,0}$ space, therefore the maximal effect for $q = 1$ depends on τ itself. For instance, this can lead to decreases in the derived fractional ages from the TAMS to about $\tau = 88\%$, from $\tau = 80\%$ to about $\tau = 55\%$, and from $\tau = 50\%$ to the ZAMS. Derived masses generally decrease over the whole course of the curves; this effect can reach up to 15% for the whole investigated mass range.

An independent test for binarity can be carried out using members of star clusters with known ages, which enables us to calculate τ for a given mass and check whether the location in the $M_{G,0}$ versus $(BP-RP)_0$ diagram matches. Unfortunately, only LAMOST J041533.86+493944.1 was identified as member of the open cluster NGC 1528, which is approximately 350 Myr old. Assuming this object to be a single star, we derive a mass of about $3.1\,M_\odot$ and a fractional age of $\tau \approx 83\%$. This is not compatible with the main-sequence lifetime of about 365 Myr for the given stellar mass. We therefore conclude that
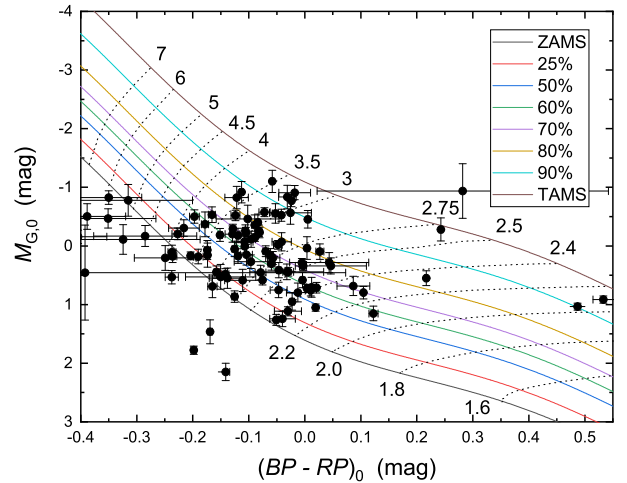
Fig. 8. $(BP-RP)_0$ versus $M_{G,0}$ diagram including lines of constant τ and masses for solar metallicity $[Z] = 0.02$.

LAMOST J041533.86+493944.1 is a binary star. Assuming $q = 0.91$, we obtain $M = 2.8\,M_\odot$ and $\tau = 73\%$, in perfect agreement with the values derived from photometry.

Taking the above discussed aspects into account, it becomes obvious that the impact of binarity on the results is significant and cannot be ignored. However, with the available data, we are not able to investigate this issue in more detail. In consequence, because of the background of the expected high percentage of binary systems among our sample stars, no individual τ and mass values were determined. As general conclusions from our analysis, we find that the investigated CP3 stars cover the whole age range from ZAMS to TAMS and are almost homogeneously distributed at fractional ages of $\tau \leq 80\%$.

3.4. Photometric variability

CP3 stars were initially regarded as being among the "quietest" (i.e. non-variable) early-type stars (Adelman 1998). With the advent of high-precision space photometry, this picture has recently been changing. However, open questions as to the involved variability mechanisms (pulsation versus rotation) remain (cf. Sect. 1). We took advantage of the new sample of CP3 stars to identify variables using data from various photometric surveys. The following sections provide an overview over the employed data sources and shortly discuss the variable stars.

3.4.1. Data sources

For the investigation of the variability of our sample stars, photometric time series data from the following survey sources were employed.

ASAS-3 (Pojmański 2002). Two wide-field telescopes equipped with f/2.3 200 mm Minolta lenses and 2048×2048 AP 10 Apogee detectors, situated at Las Campanas Observatory, Chile; V band light curves available for the entire southern sky up to $\delta < +28°$; time baseline of almost 10 yr; ASAS-3 archive[7] contains photometry for stars in the magnitude range of $7 \lesssim V \lesssim 14$.

ASAS-SN (Shappee et al. 2014; Kochanek et al. 2017). Observations obtained at five stations, each consisting of four

---

[7] http://www.astrouw.edu.pl/asas/

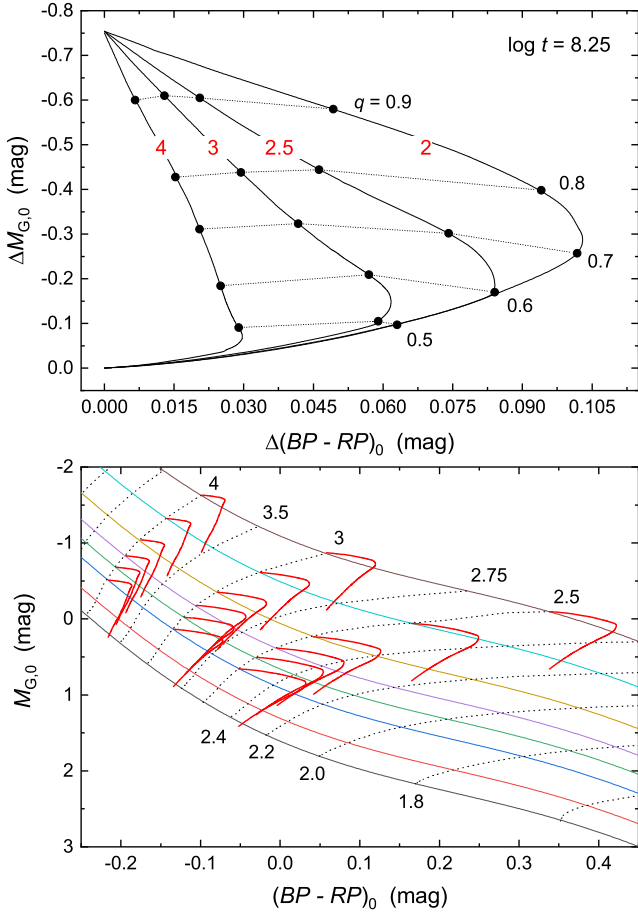**Fig. 9.** *Upper panel*: grids for different *q* values, as calculated for primary masses of 4, 3, 2.5, and 2 $M_\odot$ using an isochrone for $\log t = 8.25$. *Lower panel*: effect of binarity for different masses in the $(BP-RP)_0$ versus $M_{G,0}$ diagram.

14 cm aperture Nikon telephoto lenses equipped with *V* (two stations) or *g* (three stations) band filters[8]; entire visible sky is monitored every night to $V \lesssim 17$ mag; saturation limit 10 to 11 mag (*V*); ongoing survey, time baseline of up to six years.

Kepler prime mission/K2 (Borucki et al. 2010; Koch et al. 2010). Prime mission operational from 2009 (May 2) until 2013 (May 8); after the loss of two reaction wheels, the mission (now called K2) was changed to observe the ecliptic plane (Howell et al. 2014); differential photometer with 0.95 m aperture; detectors made up of 21 modules each equipped with 2200×1024 pixel CCD detectors; single-passband (420−900 nm) light curves taken in long-cadence (29.5 min) and short-cadence (58.5 s) modes; only PDC flux long-cadence data from the Mikulski Archive for Space Telescopes (MAST)[9] have been employed in this study.

SWASP (Pollacco et al. 2006; Butters et al. 2010). Two robotic telescopes situated at the Observatorio del Roque de los Muchachos, La Palma, and the South African Astronomical Observatory; each telescope consists of an array of eight f/1.8 200 mm Canon lenses and 2048×2048 Andor CCD detectors; observing cadence 9 to 12 min; observations unfiltered (prior to 2006) and obtained through a broadband filter (400−700 nm;

after 2006); single data release[10] contains light curves from 2004 to 2008 and provides good photometry in the magnitude range of $8 \lesssim V \lesssim 14$.

TESS (Ricker et al. 2014, 2015; Campante et al. 2016). Ongoing two-year all-sky survey aiming at the discovery of transiting exoplanets[11]; detectors consisting of four MIT/Lincoln Lab CCDs with 4096×4096 pixels (imaging area of 2048×2048 pixels; remaining pixels are used as a frame-store to allow rapid shutterless readout); cameras have an effective aperture size of 10 cm and are equipped with f/1.4 lenses; single-passband (600−1000 nm) light curves; time sampling of 2 min.

3.4.2. Photometric variables

We identified eight photometric variable CP3 stars in the accuracy limits of the employed data sources. All variables were discovered in satellite-based data. The observed peak-to-peak amplitudes are so small that the variability would probably not have been detected in ground-based observations. Corresponding light curves and frequency spectra are shown, respectively, in Figs. 10 and 11. Periods and uncertainties are provided in Table 4. Upper limits of variability for the non-variable sources are provided in Table A.2.

LAMOST J050338.55+234349.5 (HD 285110; EPIC 247702533; MKCLASS final type: B8 IV (HgMn)). This star is announced here as variable star for the first time. Based on analysis of *Kepler* K2 data, we derive a period of $P = 2.99(2)$ d and a peak-to-peak variability amplitude of 0.0023 mag ($K_{\rm p}$). Only one significant period and corresponding harmonics are present in the Fourier spectrum, which is in line with rotational modulation. The light curve shows some irregularities, which are likely of instrumental origin.

LAMOST J060937.73+235218.0 (HD 252428; EPIC 202060532; MKCLASS final type: B8 III–IV HgMn). This star was identified as a photometric variable on the basis of *Kepler* K2 data by Armstrong et al. (2016), who derived a period of $P = 9.901513$ d and a peak-to-peak variability amplitude of 0.002 mag ($K_{\rm p}$). No variability type was specified. Based on this information, the star is listed as variable star of unspecified type (type VAR) in the International Variable Star Index (VSX) of the American Association of Variable Star Observers (AAVSO; Watson 2006). However, the K2 data cannot be phased correctly with the period presented by Armstrong et al. (2016), which is obviously wrong. From analysis of the same dataset, we derive a period of $P = 11.44(39)$ d (peak-to-peak variability amplitude of 0.0018 mag ($K_{\rm p}$)), in agreement with the results of Balona (2016), who derived a period of 11.91(7) d for this star. The monoperiodic nature and the period of the variability suggest rotational variability but only three cycles have been covered, so more observations are needed.

LAMOST J061137.11+254307.8 (TYC 1881-804-1; EPIC 202064179; MKCLASS final type: B8 IV–V HgMn). Based on analysis of *Kepler* K2 data, this star was announced as a variable star of unspecified type by Armstrong et al. (2015), who gave a period of $P = 6.248527$ d and derived a peak-to-peak variability amplitude of 0.007 mag ($K_{\rm p}$). Balona (2016) investigated the same dataset and derived a period of 6.33(5) d. Our period solution ($P = 6.2(3)$ d; peak-to-peak variability amplitude of 0.0028 mag ($K_{\rm p}$)) agrees with the above mentioned literature

---
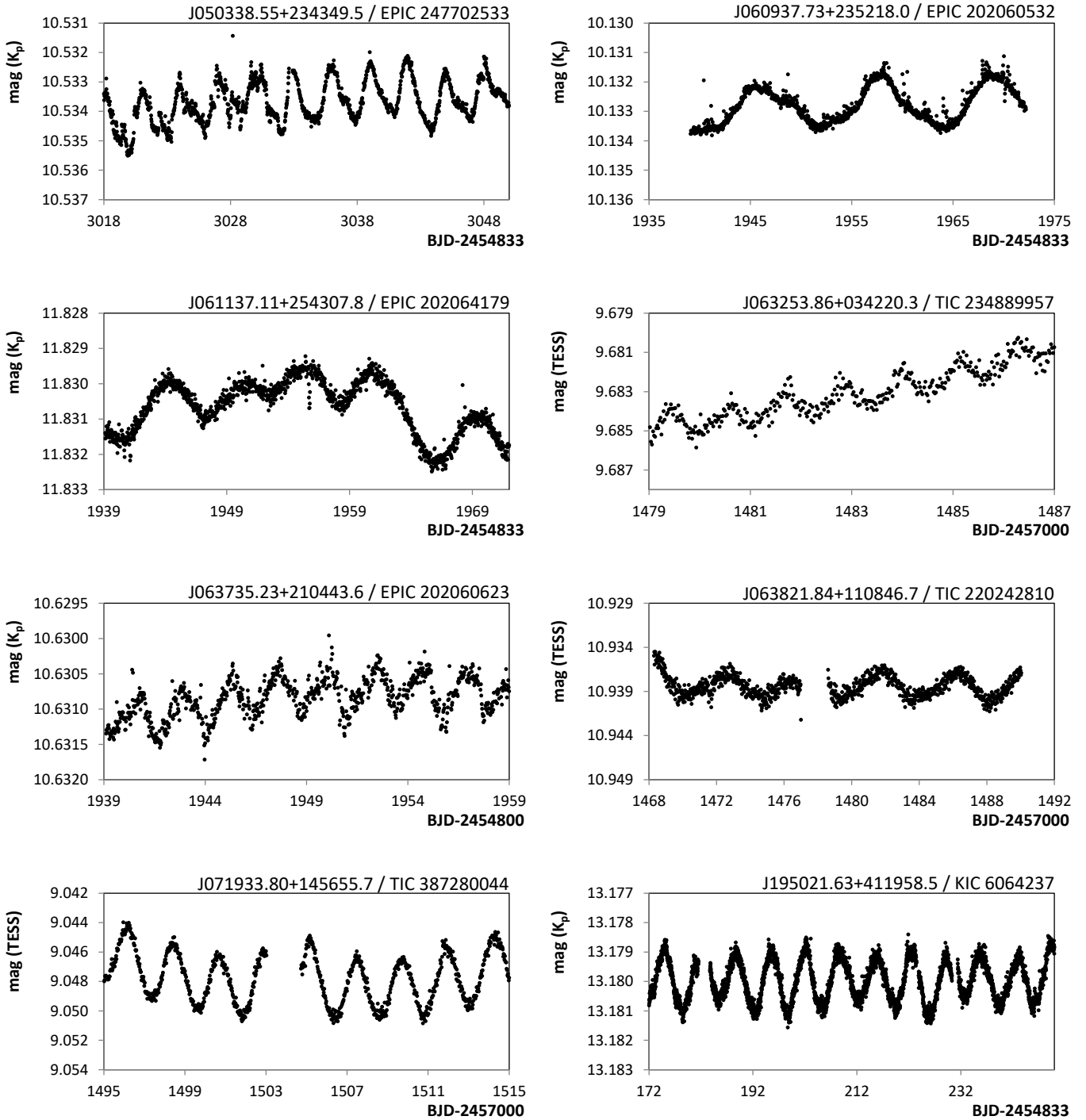
Fig. 10. Representative parts of the light curves of the eight CP3 stars identified as photometric variables in this study. Identifiers are indicated in the panels.

results. The star shows an interesting light curve and is obviously multi-periodic. We consider it a prime target for further studies aimed at deciphering the variability mechanisms at work in CP3 stars.

LAMOST J063253.86+034220.3 (HD 46338; TIC 234889 957; MKCLASS final type: B8 V (HgMn)). Based on analysis of TESS data, we here identify this star as a new variable star and derive a period of $P = 1.14(1)$ d and a peak-to-peak variability amplitude of 0.0014 mag (TESS). The monoperiodic nature of the light variability suggests rotational modulation. There is an

obvious long-term trend in brightness, which may be of instrumental origin.

LAMOST J063735.23+210443.6 (HD 260690; EPIC 2020 60623; MKCLASS final type: B9 III–IV HgMn). This star was announced as a variable star on the basis of *Kepler* K2 data by Armstrong et al. (2015), who derived a period of $P = 2.38192$ d and a peak-to-peak variability amplitude of 0.002 mag ($K_{\rm p}$). Balona (2016) derived a slightly but significantly different period of $P = 2.364(3)$ d, which, nevertheless, agrees with our period solution of $P = 2.34(2)$ d (peak-to-peak variability amplitude of
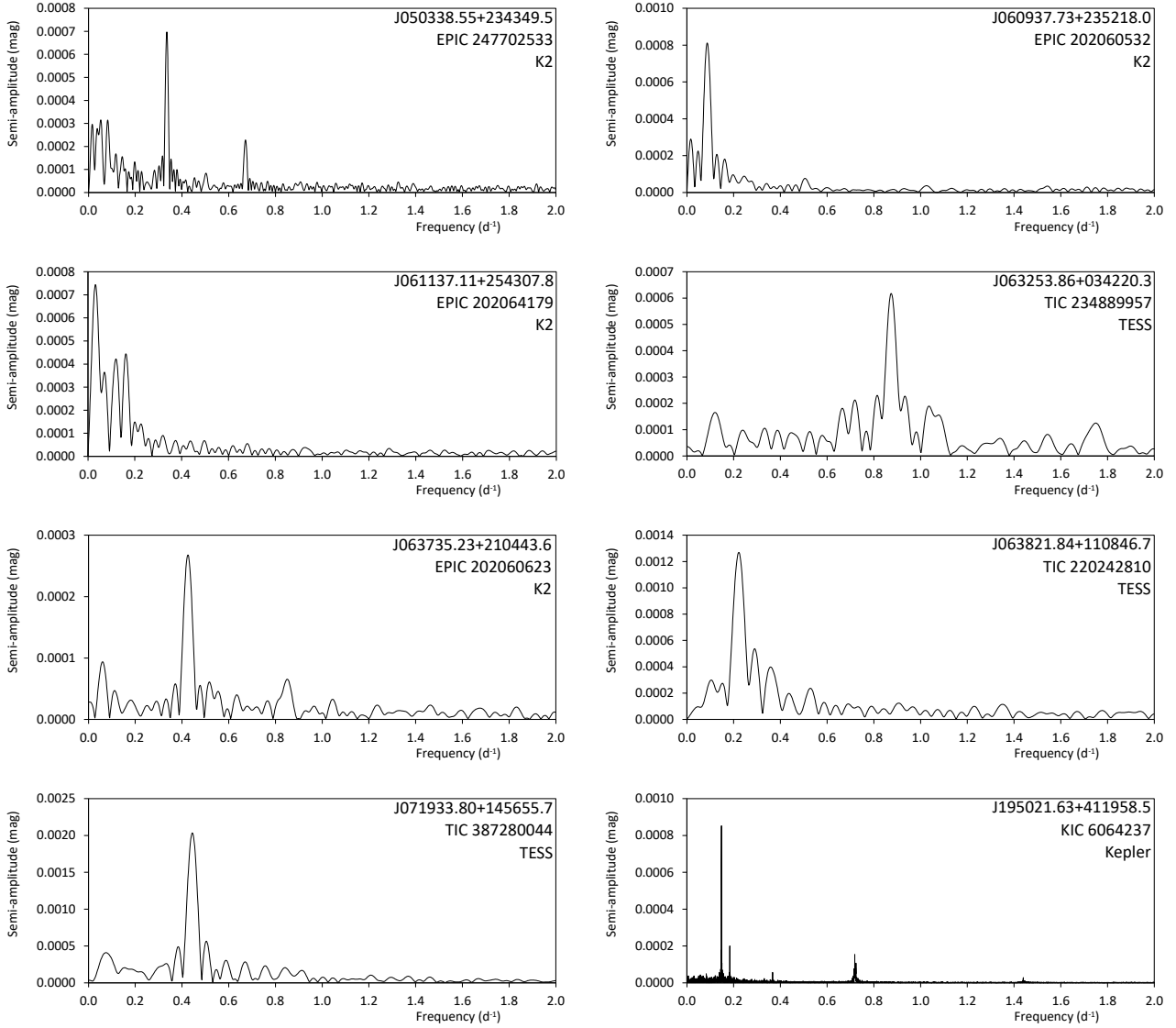
Fig. 11. Fourier spectra of the eight CP3 stars identified as photometric variables in this study. Identifiers and data sources are indicated in the panels.

0.0007 mag (K_p)). The observed monoperiodic variability and the presence of harmonic frequencies are in agreement with rotational modulation.

LAMOST J063821.84+110846.7 (HD 261050; TIC 220242 810; MKCLASS final type: B8 III HgMn). Based on analysis of TESS data, we here identify this star as a new variable star and derive a period of $P = 4.47(14)$ d and a peak-to-peak variability amplitude of 0.0036 mag (TESS). The monoperiodic nature of the light variability suggests rotational modulation.

LAMOST J071933.80+145655.7 (HD 56914; TIC 387280 044; MKCLASS final type: B8 IV HgMn). Based on analysis of TESS data, we here identify this star as a new variable star and derive a period of $P = 2.25(3)$ d and a peak-to-peak variability amplitude of 0.0042 mag (TESS). The monoperiodic nature of the light variability suggests rotational modulation.

LAMOST J195021.63+411958.5 (Gaia DR2 20768736 34046444800; KIC 6064237; MKCLASS final type: B9 IV HgMn). This star was first identified as a photometric variable on the basis of *Kepler* Q1 data by Debosscher et al. (2011). It has been proposed as a rotational variable in the literature

(Balona 2013; Nielsen et al. 2013). From analysis of the full *Kepler* dataset, we derive a main period of $P = 6.7675(4)$ d and a peak-to-peak variability amplitude of 0.0024 mag (K_p), in agreement with the results from former investigations ($P = 6.757$ d, Balona 2013; $P = 6.768$ d, Nielsen et al. 2013). Interestingly, the star is obviously multi-periodic. We identify 11 independent and highly significant ($S/N > 7$) frequencies, which are listed in Table 5. The star is therefore a prime candidate for further studies as well as asteroseismological and pulsational modelling attempts.

4. Conclusions

Using an altered version of Richard O. Gray's MKCLASS code, which was tailored to probe several Hg II and Mn II features relevant to the identification of CP3 stars, we searched for CP3 stars among the LAMOST DR4 spectra of a colour-preselected sample of early-type stars. The spectra of all selected candidates were visually inspected; non-CP3 objects were sorted out and the strength of the Hg II and Mn II features was estimated. Depending on this estimate, the resulting sample was divided

Table 4. Periods of the eight photometric variable CP3 stars identified in this study.

(1) ID_LAMOST	(2) P_{our} (d)	(3) P_{lit} (d)
J050338.55+234349.5	2.99(2)	–
J060937.73+235218.0	11.44(39)	9.901513 [a], 11.91(7) [b]
J061137.11+254307.8	6.2(3) [1]	6.248527 [a], 6.33(5) [b]
J063253.86+034220.3	1.14(1)	–
J063735.23+210443.6	2.34(2)	2.38192 [a], 2.364(3) [b]
J063821.84+110846.7	4.47(14)	–
J071933.80+145655.7	2.25(3)	–
J195021.63+411958.5	6.7675(4) [1]	6.757 [c], 6.768 [d]

Notes. The columns denote: (1) LAMOST identifier. (2) Period derived in this study. (3) Literature period. The corresponding references are indicated in the notes. [1]Multi-periodic. **References.** [a]Armstrong et al. (2016), [b]Balona (2016), [c]Balona (2013), [d]Nielsen et al. (2013).

Table 5. Frequency solution for KIC 6064237.

(1) No.	(2) Frequency	(3) Semiamplitude	(4) Phase	(5) Remark
f_1	0.147770	0.000859	0.383	
f_2	0.183330	0.000197	0.327	
f_3	0.718329	0.000171	0.277	
f_4	0.723315	0.000119	0.874	
f_5	0.719782	0.000096	0.248	
f_6	0.715784	0.000080	0.467	
f_7	0.722585	0.000082	0.179	
f_8	0.720130	0.000095	0.308	
f_9	0.366583	0.000054	0.044	$2f_2$
f_{10}	0.721365	0.000058	0.045	
f_{11}	0.030432	0.000034	0.006	Sidereal period?

Notes. The columns denote: (1) Frequency identification. (2) Frequency (d^{-1}). (3) Semiamplitude. (4) Phase, as derived with PERIOD04 (reference time = BJD−2454833). (5) Remark.

into bona fide CP3 stars, good CP3 star candidates, and candidates.

The main findings of the present investigation are summarised in the following:

– We present 99 bona fide CP3 stars, 19 good CP3 star candidates, and seven candidates. Most of these stars are new discoveries (only 15 stars are contained in the catalogue of Chojnowski et al. 2020). The resulting increased sample size of CP3 stars will greatly benefit in-depth statistical studies.
– In accordance with the expectations for CP3 stars, all our sample stars are contained within the narrow spectral temperature-type range from B6 to B9.5. This is in excellent agreement with the derived mass estimates, which denote masses between $2.4\,M_\odot$ and $4\,M_\odot$ for most of our sample stars, which are mostly between 100 Myr and 500 Myr old.
– With a broad peak distribution between G magnitudes 9.5 and 13.5, the sample presented here contains on average the faintest CP3 stars known, forming a perfect extension to the samples of Renson & Manfroid (2009) and Chojnowski et al. (2020).
– Our sample stars cover the whole age range from ZAMS to TAMS and are almost homogeneously distributed at

fractional ages of $\tau \le 80\%$, with an apparent accumulation of objects between $50\% < \tau < 80\%$.
– Using various indirect indicators of multiplicity, we find that only 12 objects (or 8% of our sample) show no indication of binarity, in agreement with the expectation for this group of objects.
– We investigate the impact of binarity on the mass and age estimates and find it to be significant. We are, however, unable to investigate this issue in more detail with the available data. Because of the background of the expected high percentage of binary systems among our sample stars, no individual τ and mass values were determined. We caution that it is imperative that the effects of binarity are taken into account when determining the mass and age of any sample of CP3 stars.
– Using time series data from diverse photometric surveys, we investigate the photometric variability of our sample stars. Only eight photometric variables were discovered. Most of these stars show monoperiodic variability in agreement with rotational modulation. LAMOST J061137.11+254307.8 and LAMOST J195021.63+411958.5 show multi-periodic variability and are prime candidates for additional studies dealing with the origin of the photometric variability of this group of CP stars as well as asteroseismological and pulsational modelling attempts.

Future investigations will be concerned with expanding the approach presented here to other massive spectral databases, in order to further increase the sample size of Galatic CP3 stars.

References

Adelman, S. J. 1998, A&AS, 132, 93
Adelman, S. J., Gulliver, A. F., Kochukhov, O. P., & Ryabchikova, T. A. 2002, ApJ, 575, 449
Alecian, G. 2012, in Progress in Solar/Stellar Physics with Helio- and Asteroseismology, eds. H. Shibahashi, M. Takata, & A. E. Lynas-Gray, ASP Conf. Ser., 462, 80
Alecian, G. 2013, in Progress in Physics of the Sun and Stars: A New Era in Helio- and Asteroseismology, eds. H. Shibahashi, & A. E. Lynas-Gray, ASP Conf. Ser., 479, 35
Alecian, G., & Stift, M. J. 2017, MNRAS, 468, 1023
Alecian, G., & Stift, M. J. 2019, MNRAS, 482, 4519
Alecian, G., Gebran, M., Auvergne, M., et al. 2009, A&A, 506, 69
Ammons, S. M., Robinson, S. E., Strader, J., et al. 2006, ApJ, 638, 1004
Arenou, F., Luri, X., Babusiaux, C., et al. 2018, A&A, 616, A17
Armstrong, D. J., Kirk, J., Lam, K. W. F., et al. 2015, A&A, 579, A19
Armstrong, D. J., Kirk, J., Lam, K. W. F., et al. 2016, MNRAS, 456, 2260
Bagnulo, S., Landstreet, J. D., Mason, E., et al. 2006, A&A, 450, 777
Bai, Y., Liu, J., Wicker, J., et al. 2018, ApJS, 235, 16
Bai, Y., Liu, J., Bai, Z., Wang, S., & Fan, D. 2019, AJ, 158, 93

Bailer-Jones, C. A. L., Rybizki, J., Fouesneau, M., Mantelet, G., & Andrae, R. 2018, AJ, 156, 58
Balona, L. A. 2013, MNRAS, 431, 2240
Balona, L. A. 2016, MNRAS, 457, 3724
Boch, T., & Fernique, P. 2014, in Astronomical Data Analysis Software and Systems XXIII, eds. N. Manset, & P. Forshay, ASP Conf. Ser., 485, 277
Bonnarel, F., Fernique, P., Bienaymé, O., et al. 2000, A&AS, 143, 33
Borucki, W. J., Koch, D., Basri, G., et al. 2010, Science, 327, 977
Bressan, A., Marigo, P., Girardi, L., et al. 2012, MNRAS, 427, 127
Briquet, M., Korhonen, H., González, J. F., Hubrig, S., & Hackman, T. 2010, A&A, 511, A71
Butters, O. W., West, R. G., Anderson, D. R., et al. 2010, A&A, 520, L10
Campante, T. L., Schofield, M., Kuszlewicz, J. S., et al. 2016, ApJ, 830, 138
Cantat-Gaudin, T., Jordi, C., Vallenari, A., et al. 2018, A&A, 618, A93
Castelli, F., & Hubrig, S. 2004, A&A, 425, 263
Castelli, F., & Kurucz, R. L. 2003, in Modelling of Stellar Atmospheres, eds. N. Piskunov, W. W. Weiss, & D. F. Gray, IAU Symp., 210, A20
Chojnowski, S. D., Hubrig, S., Hasselquist, S., et al. 2020, MNRAS, 496, 832
Cowley, C. R., & Aikman, G. C. L. 1975, PASP, 87, 513
Cui, X.-Q., Zhao, Y.-H., Chu, Y.-Q., et al. 2012, Res. Astron. Astrophys., 12, 1197
Debosscher, J., Blomme, J., Aerts, C., & De Ridder, J. 2011, A&A, 529, A89
Gaia Collaboration (Prusti, T., et al.) 2016, A&A, 595, A1
Gaia Collaboration (Brown, A. G. A., et al.) 2018, A&A, 616, A1
Geier, S. 2020, A&A, 635, A193
Ghazaryan, S., & Alecian, G. 2016, MNRAS, 460, 1912
Ghazaryan, S., Alecian, G., & Hakobyan, A. A. 2018, MNRAS, 480, 2953
Gray, R. O., & Corbally, C. J. 1994, AJ, 107, 742
Gray, R. O., & Corbally, C. J. 2009, Stellar Spectral Classification (Princeton: Princeton University Press)
Gray, R. O., & Corbally, C. J. 2014, AJ, 147, 80
Gray, R. O., Corbally, C. J., De Cat, P., et al. 2016, AJ, 151, 13
Green, G. M., Schlafly, E. F., Finkbeiner, D., et al. 2018, MNRAS, 478, 651
Guthrie, B. N. G. 1971, Ap&SS, 10, 156
Heber, U. 2016, PASP, 128, 082001
Hou, W., Luo, A., Yang, H., et al. 2015, MNRAS, 449, 1401
Howell, S. B., Sobeck, C., Haas, M., et al. 2014, PASP, 126, 398
Hubrig, S., & Mathys, G. 1995, Comments Astrophys., 18, 167
Hubrig, S., González, J. F., Savanov, I., et al. 2006, MNRAS, 371, 1953
Hubrig, S., Savanov, I., Ilyin, I., et al. 2010, MNRAS, 408, L61
Hubrig, S., González, J. F., Ilyin, I., et al. 2012, A&A, 547, A90
Hubrig, S., Järvinen, S. P., Korhonen, H., et al. 2020, MNRAS, 495, L97
Hümmerich, S., Niemczura, E., Walczak, P., et al. 2018, MNRAS, 474, 2467
Hümmerich, S., Paunzen, E., & Bernhard, K. 2020, A&A, 640, A40
Kharchenko, N. V., Piskunov, A. E., Schilbach, E., Röser, S., & Scholz, R. D. 2013, A&A, 558, A53
Koch, D. G., Borucki, W. J., Basri, G., et al. 2010, ApJ, 713, L79
Kochanek, C. S., Shappee, B. J., Stanek, K. Z., et al. 2017, PASP, 129, 104502
Kochukhov, O., Adelman, S. J., Gulliver, A. F., & Piskunov, N. 2007, Nat. Phys., 3, 526
Kochukhov, O., Makaganiuk, V., Piskunov, N., et al. 2013, A&A, 554, A61
Korhonen, H., González, J. F., Briquet, M., et al. 2013, A&A, 553, A27
Kupka, F., Piskunov, N., Ryabchikova, T. A., Stempels, H. C., & Weiss, W. W. 1999, A&AS, 138, 119
Loden, L. O., & Sundman, A. 1987, JApA, 8, 351
Luo, A. L., Zhao, Y. H., Zhao, G., et al. 2018, VizieR Online Data Catalog: V/153
Mathys, G. 2004, in Stellar Rotation, eds. A. Maeder, & P. Eenens, IAU Symp., 215, 270
Michaud, G. 1970, ApJ, 160, 641
Monier, R., Griffin, E., Gebran, M., et al. 2019, AJ, 158, 157
Monier, R., Niemczura, E., & Kılıçoğlu, T. 2020, Res. Notes Am. Astron. Soc., 4, 48
Murphy, S. J., & Paunzen, E. 2017, MNRAS, 466, 546
Naslim, N., Jeffery, C. S., Behara, N. T., & Hibbert, A. 2011, MNRAS, 412, 363
Nielsen, M. B., Gizon, L., Schunker, H., & Karoff, C. 2013, A&A, 557, L10
Paunzen, E. 2015, A&A, 580, A23
Paunzen, E., Netopil, M., Pintado, O. I., & Rode-Paunzen, M. 2011, Astron. Nachr., 332, 77
Pelisoli, I., Bell, K. J., Kepler, S. O., & Koester, D. 2019, MNRAS, 482, 3831
Pojmański, G. 2002, Acta Astron., 52, 397
Pollacco, D. L., Skillen, I., Collier Cameron, A., et al. 2006, PASP, 118, 1407
Preston, G. 1973, Nucl. Instrum. Meth., 110, 405
Preston, G. W. 1974, ARA&A, 12, 257
Qin, L., Luo, A. L., Hou, W., et al. 2019, ApJS, 242, 13
Renson, P., & Manfroid, J. 2009, A&A, 498, 961
Richer, J., Michaud, G., & Turcotte, S. 2000, ApJ, 529, 338
Ricker, G. R., Winn, J. N., Vanderspek, R., et al. 2014, in Transiting Exoplanet Survey Satellite (TESS), SPIE Conf. Ser., 9143, 914320
Ricker, G. R., Winn, J. N., Vanderspek, R., et al. 2015, J. Astron. Telesc. Instrum. Syst., 1, 014003
Ryabchikova, T. 1998, Contrib. Astron. Obs. Skaln. Pleso, 27, 319
Schöller, M., Correia, S., Hubrig, S., & Ageorges, N. 2010, A&A, 522, A85
Shappee, B. J., Prieto, J. L., Grupe, D., et al. 2014, ApJ, 788, 48
Smith, M. A. 1974, ApJ, 189, 101
Smith, K. C. 1996, Ap&SS, 237, 77
Stassun, K. G., Oelkers, R. J., Paegert, M., et al. 2019, AJ, 158, 138
Turcotte, S., & Richard, O. 2003, Ap&SS, 284, 225
Vagnozzi, S. 2019, Atoms, 7, 41
Wahlgren, G. M., & Dolk, L. 1998, Contrib. Astron. Obs. Skaln. Pleso, 27, 314
Watson, C. L. 2006, Soc. Astron. Sci. Annu. Symp., 25, 47
Xiang, M., Ting, Y.-S., Rix, H.-W., et al. 2019, ApJS, 245, 34
Zavada, P., & Píška, K. 2020, AJ, 159, 33
Zhao, G., Zhao, Y.-H., Chu, Y.-Q., Jing, Y.-P., & Deng, L.-C. 2012, Res. Astron. Astrophys., 12, 723

Appendix A: Essential data for our sample stars

Table A.1 lists essential data for our sample stars. It is organised as follows:

- Column 1: Internal identification number.
- Column 2: LAMOST identifier.
- Column 3: Alternativ identifier (HD number, TYC identifier, or *Gaia* DR2 number).
- Column 4: Right ascension (J2000). Positional information was taken from *Gaia* DR2 (Gaia Collaboration 2018; Arenou et al. 2018).
- Column 5: Declination (J2000).
- Column 6: MKCLASS final type, as derived in this study[12].
- Column 7: Sloan *g* band S/N of the analysed spectrum.
- Column 8: *G* mag (*Gaia* DR2).
- Column 9: *G* mag error.
- Column 10: Parallax (*Gaia* DR2).
- Column 11: Parallax error.
- Column 12: Dereddened colour index $(BP-RP)_0$ (*Gaia* DR2).
- Column 13: Colour index error.
- Column 14: Absorption in the *G* band, A_G.
- Column 15: Intrinsic absolute magnitude in the *G* band, $M_{G,0}$.
- Column 16: Absolute magnitude error.

Upper limits of variability are provided in Table A.2.

---

[12] We note that, as in the Renson & Manfroid (2009) catalogue, the "*p*" denoting peculiarity was omitted from the spectral classifications.

Table A.1. Essential data for our sample stars, sorted by increasing right ascension.

(1) No.	(2) ID_LAMOST	(3) ID_alt	(4) RA(J2000)	(5) Dec(J2000)	(6) SpT_final	(7) S/N g	(8) G mag	(9) e_G mag	(10) pi (mas)	(11) e_pi	(12) $(BP-RP)_0$	(13) $e\_(BP-RP)_0$	(14) A_G	(15) M_{G0}	(16) e_M_{G0}
1	J000118.65+464355.0	HD 224872	00 01 19.00	+46 43 55.01	B9.5 III HgMn	316	8.2905	0.0005	2.2517	0.0676	−0.089	0.002	0.197	−0.144	0.065
2	J002635.94+562206.5	TYC3661-39-1	00 26 35.91	+56 22 06.63	B9 IV−V HgMn	250	11.2054	0.0011	0.6004	0.0593	−0.102	0.056	0.557	−0.459	0.236
3	J020922.72+533908.6	TYC3685-766-1	02 09 22.74	+53 39 06.99	B8 IV HgMn	270	10.4932	0.0003	0.7401	0.0514	+0.005	0.003	0.294	−0.455	0.151
4	J030852.02+553734.3	TYC3706-249-1	03 08 52.03	+55 37 34.35	B8 IV HgMn	157	11.1172	0.0005	1.5127	0.0357	+0.533	0.019	1.102	+0.914	0.060
5	J031312.82+493559.8	TYC3319-890-1	03 13 12.72	+49 35 59.76	B9 III−IV HgMn	216	10.9302	0.0003	–	–	–	–	0.767	–	–
6	J031943.49+561329.7	TYC3706-265-1	03 19 43.49	+56 13 29.74	B7 III HgMn	215	11.0004	0.0005	0.8892	0.0632	+0.282	0.260	1.681	−0.935	0.465
7	J032252.69+582806.7	TYC3715-493-1	03 22 52.69	+58 28 06.69	B6 IV HgMn	170	11.5315	0.0005	1.0023	0.0342	−0.351	0.085	2.005	−0.469	0.163
8	J033700.61+571139.0	TYC3724-347-1	03 37 00.37	+57 11 39.56	B9 IV (HgMn)	164	10.4069	0.0014	3.9697	0.4858	−0.689	0.040	0.126	+3.274	0.275
9	J033939.69+473758.3	TYC3317-2031-1	03 39 39.69	+47 37 58.36	B8 IV HgMn	178	11.1676	0.0007	0.8508	0.0353	−0.081	0.003	1.047	−0.230	0.090
10	J034903.76+454037.3	TYC3326-1800-1	03 49 03.77	+45 40 37.48	B9 IV HgMn	619	10.1595	0.0011	2.0305	0.0575	+0.019	0.002	0.646	+1.051	0.061
11	J035332.73+523248.9	Gaia DR2251948416582201600	03 53 32.74	+52 32 48.91	B9 V HgMn	243	12.0045	0.0002	1.1101	0.0332	−0.030	0.024	1.118	+1.113	0.077
12	J035333.90+524118.7	TYC3717-313-1	03 53 33.91	+52 41 18.64	B9 IV HgMn	311	11.3319	0.0008	0.9816	0.0470	−0.096	0.030	1.022	+0.269	0.116
13	J035805.60+452213.6	TYC3327-113-1	03 58 05.60	+45 22 13.66	B8 IV HgMn	363	10.9552	0.0007	1.2487	0.0438	−0.003	0.006	1.096	+0.341	0.077
14	J040155.24+514923.5	TYC3339-14-1	04 01 55.23	+51 49 25.54	B8 V HgMn	219	10.4772	0.0005	1.3808	0.0438	−0.032	0.066	0.736	+0.442	0.135
15	J040437.83+460141.5	TYC3327-946-1	04 04 37.84	+46 01 41.51	B9 IV HgMn	252	11.2340	0.0009	1.1841	0.0603	−0.059	0.006	1.298	+0.303	0.111
16	J041102.63+513103.7	TYC3340-532-1	04 11 02.64	+51 31 03.70	B8 V HgMn	190	11.6903	0.0006	0.7446	0.0553	−0.174	0.005	0.979	+0.071	0.161
17	J041115.00+360322.2	Gaia DR2177165618554221312	04 11 15.01	+36 03 22.24	B9 II−III HgMn	209	12.1073	0.0002	0.3783	0.0490	−0.122	0.004	0.879	−0.882	0.281
18	J041446.58+454448.3	TYC3328-1424-1	04 14 46.58	+45 44 48.40	B9.5 III HgMn	344	11.2415	0.0010	0.9165	0.0549	+0.027	0.007	0.955	−0.097	0.131
19	J041533.86+493944.1 [a]	TYC3336-762-1	04 15 34.12	+49 39 45.54	B8 IV HgMn	429	9.8972	0.0005	1.2322	0.0410	−0.072	0.010	0.926	−0.576	0.074
20	J041632.64+424344.2	Gaia DR2229032193375251328	04 16 32.64	+42 43 44.31	B8 V (HgMn)	175	12.1332	0.0003	0.6091	0.0551	+0.243	0.003	1.338	−0.282	0.196
21	J042204.78+482811.3	Gaia DR2258829381053351552	04 22 04.79	+48 28 11.42	B8 IV (HgMn)	121	12.2792	0.0002	0.8299	0.0316	+0.046	0.063	1.535	−0.339	0.137
22	J042726.80+525506.2	TYC3732-1016-1	04 27 26.82	+52 55 06.22	B8 IV−V HgMn	562	10.1456	0.0004	1.4293	0.0495	−0.285	0.092	1.091	−0.169	0.178
23	J042829.12+511637.5	HD 232961	04 28 28.81	+51 16 37.58	B8 IV−V HgMn	397	9.8120	0.0005	1.7241	0.0597	−0.324	0.137	1.105	−0.110	0.252
24	J042908.75+530654.3	Gaia DR2272149949877398400	04 29 08.75	+53 06 54.31	B9 III−IV HgMn	174	12.1482	0.0002	1.0128	0.0335	−0.030	0.010	1.734	+0.441	0.074
25	J043338.55+523755.1 [a]	HD 232975	04 33 38.89	+52 37 55.13	B8 IV−V HgMn	348	9.5673	0.0002	1.7266	0.0413	−0.350	0.059	1.578	−0.825	0.114
26	J043743.94+414133.8 [a]	HD 276610	04 37 43.94	+41 41 33.81	B8 IV HgMn	247	10.2297	0.0003	0.9607	0.0451	−0.042	0.002	0.666	−0.524	0.102
27	J044429.05+554643.2	Gaia DR2274518164783721472	04 44 29.06	+55 46 43.19	B8 IV HgMn	113	13.1855	0.0003	0.3542	0.0249	−0.041	0.017	1.001	−0.070	0.155
28	J044732.75+482124.5	TYC3347-1290-1	04 47 32.76	+48 21 24.54	B8 IV HgMn	189	10.5235	0.0004	1.1015	0.0498	−0.227	0.010	0.939	−0.205	0.100
29	J045516.12+581945.5	TYC3746-129-1	04 55 16.12	+58 19 45.62	B8 IV−V HgMn	366	10.3948	0.0004	1.6412	0.0433	−0.487	0.007	0.436	+1.035	0.058
30	J050338.55+234349.5	HD 285110	05 03 38.57	+23 43 49.67	B8 IV (HgMn)	222	10.6501	0.0005	1.5336	0.0694	+0.010	0.003	0.823	+0.756	0.098
31	J050740.17+380705.1	TYC2895-2440-1	05 07 40.17	+38 07 05.03	B8 IV HgMn	125	11.5741	0.0005	1.1917	0.0469	−0.076	0.003	1.374	+0.581	0.086
32	J050810.73+453321.8 [a]	TYC3345-3314-1	05 08 10.81	+45 33 22.70	B8 III−IV HgMn	210	10.7819	0.0004	0.8520	0.0482	−0.119	0.003	0.612	−0.178	0.123
33	J051309.48+551742.2	TYC3739-643-1	05 13 09.49	+55 17 42.26	B9 III−IV HgMn	192	11.0260	0.0007	1.1686	0.0662	−0.061	0.005	1.197	−0.167	0.123
34	J051503.39+323903.2	Gaia DR2180704873465298432	05 15 03.39	+32 39 03.24	B7 IV−V (HgMn:)	140	12.1514	0.0004	0.7300	0.0607	−0.111	0.032	0.881	+0.587	0.189
35	J051625.06+563321.2	TYC3743-51-1	05 16 25.10	+56 33 21.33	B7 IV−V HgMn	128	11.0038	0.0007	1.1158	0.0375	−0.048	0.008	1.261	−0.019	0.074
36	J051813.77+452059.7	TYC3358-979-1	05 18 13.77	+45 20 59.77	B8 III−IV HgMn	279	11.2963	0.0010	0.5462	0.0460	−0.113	0.003	0.901	−0.917	0.183
37	J052056.26+085723.5	HD 242852	05 20 56.27	+08 57 23.53	B8 IV HgMn	241	10.1233	0.0006	1.6486	0.0734	−0.105	0.002	1.427	−0.218	0.097
38	J052119.19+370619.9	Gaia DR2184455827321040896	05 21 19.20	+37 06 20.04	B9 III−IV HgMn	108	12.8334	0.0005	0.5342	0.0442	−0.150	0.063	0.945	−0.527	0.210
39	J052308.77+323128.3 [b]	HD 242991	05 23 08.78	+32 31 28.35	B9 IV−V HgMn	302	10.7273	0.0005	0.9065	0.1014	−0.150	0.003	0.614	−0.100	0.243
40	J052436.09+321553.5	HD 243231	05 24 36.10	+32 15 53.71	B7 V HgMn	328	10.6718	0.0004	1.5063	0.4506	−0.002	0.146	0.447	+1.114	0.699
41	J052606.26+321808.6	HD 243493	05 26 06.27	+32 18 08.75	B9 III HgMn	133	11.6397	0.0004	0.6341	0.0403	−0.129	0.013	0.852	−0.202	0.140
42	J052649.33+431004.9	TYC2921-1297-1	05 26 49.33	+43 10 05.00	B9 IV HgMn	267	11.3570	0.0008	0.8990	0.0645	+0.087	0.029	0.444	+0.682	0.164

Notes. The columns denote: (1) Internal identification number. (2) LAMOST identifier. (3) Alternative identifier (HD number, TYC identifier or *Gaia* DR2 number). (4) Right ascension (J2000; *Gaia* DR2). (5) Declination (J2000; *Gaia* DR2). (6) Spectral type, as derived in this study. (7) Sloan *g* band S/N of the analysed spectrum. (8) *G* mag (*Gaia* DR2). (9) *G* mag error. (10) Parallax (*Gaia* DR2). (11) Parallax error. (12) Dereddened colour index $(BP-RP)_0$ (*Gaia* DR2). (13) Colour index error. (14) Absorption in the *G* band, A_G. (15) Intrinsic absolute magnitude in the *G* band, $M_{G,0}$. (16) Absolute magnitude error. [a]Contained in the sample of APOGEE CP3 stars of Chojnowski et al. (2020). [b]Renson & Manfroid (2009): Renson 8947; spectral type: B9 Si. LAMOST spectrum shows typical signature of a CP3 star; not a classical CP2 star. [c]Renson & Manfroid (2009): Renson 10597; spectral type: B8 Si; CP star of doubtful nature. LAMOST spectrum shows typical signature of a CP3 star; not a classical CP2 star. [d]Renson & Manfroid (2009): Renson 11944; spectral type: A0; CP star of doubtful nature. LAMOST spectrum shows typical signature of a CP3 star.

Table A.1. continued.

(1) No.	(2) ID_LAMOST	(3) ID_alt	(4) RA(J2000)	(5) Dec(J2000)	(6) SpT_final	(7) S/N g	(8) Gmag	(9) e_Gmag	(10) pi (mas)	(11) e_pi	(12) $(BP-RP)_0$	(13) $e_{(BP-RP)_0}$	(14) A_G	(15) M_{G0}	(16) $e_{M_{G0}}$
43	J052746.31+314215.9	HD 243760	05 27 46.31	+31 42 15.90	B7 III–IV (HgMn:)	214	10.8051	0.0004	0.9702	0.0480	−0.108	0.015	0.810	−0.070	0.110
44	J052808.91+315213.3	HD 243806	05 28 08.91	+31 52 13.44	B8 IV HgMn	345	9.7190	0.0005	1.2846	0.1441	−0.015	0.070	0.521	−0.258	0.274
45	J053028.44+060100.9	Gaia DR2 3237727698424162304	05 30 28.44	+06 01 00.53	B9 IV–V HgMn	164	12.2845	0.0002	1.0175	0.0447	−0.051	0.003	1.061	+1.261	0.095
46	J053419.30+302407.7 [a]	HD 244826	05 34 19.08	+30 24 07.64	B7 III–IV HgMn	312	9.9475	0.0009	1.0973	0.0598	−0.018	0.028	1.058	−0.909	0.121
47	J053513.37+192705.9	TYC 1305-1903-1	05 35 13.37	+19 27 05.96	B8 IV–V HgMn	238	11.7078	0.0004	0.7565	0.0464	−0.004	0.004	0.521	−0.581	0.133
48	J053642.85+240205.8 [a]	HD 245324	05 36 42.86	+24 02 05.85	B8 IV HgMn	393	10.6003	0.0006	0.8801	0.0741	−0.315	0.115	1.101	−0.778	0.271
49	J053819.93+392350.0 [a]	TYC 2914-1196-1	05 38 20.01	+39 23 49.76	B8 IV HgMn	439	10.7991	0.0005	0.9685	0.0491	−0.151	0.004	0.917	−0.187	0.110
50	J053836.11+340929.7	TYC 2412-837-1	05 38 36.12	+34 09 29.77	B6 III (HgMn)	159	11.7727	0.0004	0.4500	0.0719	−0.073	0.045	1.111	−1.072	0.355
51	J054033.05+331124.6 [a]	HD 246021	05 40 32.87	+33 11 24.47	B8 IV HgMn	249	10.1109	0.0007	1.5457	0.0742	−0.158	0.004	0.610	+0.446	0.104
52	J054052.69+215844.5	HD 246183	05 40 52.68	+21 58 44.53	B8 V HgMn	407	9.7474	0.0008	2.2779	0.1308	−0.040	0.023	0.291	+1.244	0.131
53	J054619.47+260416.7	HD 247308	05 46 19.25	+26 04 16.76	B8 IV–IV (Hg,Mn)	229	9.4514	0.0007	1.5906	0.0828	−0.107	0.003	0.453	+0.006	0.113
54	J054927.98+302256.1	Gaia DR2 3444706261229672960	05 49 27.99	+30 22 56.20	B8 IV HgMn	128	11.9479	0.0003	0.4494	0.0380	−0.026	0.038	0.775	−0.564	0.195
55	J055005.52+152159.5	TYC 1299-1938-1	05 50 05.53	+15 21 59.56	B8 IV (HgMn)	72	11.7326	0.0004	0.5887	0.0807	−0.078	0.008	0.608	−0.026	0.298
56	J055030.45+244900.6	TYC 1866-1183-1	05 50 30.46	+24 49 00.60	B8 IV–V (Hg)Mn	174	11.5623	0.0004	0.9437	0.0487	−0.238	0.012	0.903	−0.533	0.113
57	J055116.00+420914.5	Gaia DR2 192353272589945088	05 51 16.01	+42 09 14.57	B9 IV (HgMn)	154	12.9378	0.0005	0.3581	0.0320	+0.004	0.004	0.671	−0.036	0.194
58	J055213.34+325807.7	TYC 2410-800-1	05 52 13.35	+32 58 07.76	B8 IV (HgMn:)	104	11.9385	0.0003	0.5058	0.0755	−0.048	0.008	0.506	−0.047	0.324
59	J055309.48+265424.2 [a]	HD 248667	05 53 09.49	+26 54 24.28	B7 III–IV HgMn	216	10.4620	0.0004	0.9185	0.0479	−0.197	0.009	0.778	−0.501	0.114
60	J055400.30+290112.2 [c]	TYC 1875-1748-1	05 54 00.30	+29 01 12.33	B7 III–IV HgMn	242	10.7807	0.0006	0.6908	0.0529	−0.053	0.005	0.531	−0.553	0.166
61	J055457.96+092830.5	HD 249170	05 54 57.97	+09 28 30.50	B8 IV HgMn	189	11.0284	0.0006	1.3536	0.0754	+0.044	0.071	1.402	+0.284	0.172
62	J055505.90+212949.6	Gaia DR2 3423922746981082240	05 55 05.90	+21 29 49.70	B9 IV (HgMn:)	69	13.1423	0.0004	0.4814	0.0365	−0.138	0.032	1.005	+0.550	0.174
63	J055744.95+255028.1 [a]	HD 249589	05 57 44.95	+25 50 28.13	B8 IV HgMn	280	10.2700	0.0006	1.0163	0.0620	−0.216	0.027	0.610	−0.305	0.141
64	J055811.62+303219.5	TYC 2406-2337-1	05 58 11.62	+30 32 19.56	B9 III–IV HgMn	114	12.0241	0.0004	0.8139	0.0551	−0.023	0.004	0.628	+0.949	0.147
65	J055854.37+292654.8	TYC 1875-2341-1	05 58 54.37	+29 26 54.87	B8 IV HgMn	191	11.7884	0.0003	0.3839	0.0352	−0.031	0.016	0.544	−0.834	0.201
66	J060122.46+301948.7	TYC 2419-83-1	06 01 22.46	+30 19 48.83	B8 IV (HgMn)	65	12.6351	0.0004	0.2966	0.0363	−0.035	0.036	0.645	−0.649	0.273
67	J060238.73+295105.4 [a]	HD 250569	06 02 38.74	+29 51 05.46	B8 IV–V HgMn	130	11.0837	0.0006	0.9253	0.0434	−0.236	0.007	0.736	−0.179	0.102
68	J060405.77+290624.1	Gaia DR2 3437444781498443904	06 04 05.77	+29 06 24.21	B7 IV (HgMn:)	69	12.9727	0.0005	0.4879	0.0620	+0.014	0.010	0.378	+1.037	0.276
69	J060605.43+290405.2	HD 251407	06 06 05.44	+29 04 04.94	B8 IV–V HgMn	205	10.5333	0.0006	1.0777	0.0597	−0.237	0.007	0.589	+0.106	0.121
70	J060619.07+345118.1	TYC 2427-1141-1	06 06 19.07	+34 51 18.25	B8 V HgMn	206	10.5629	0.0005	0.9602	0.0808	−0.389	0.069	0.978	−0.503	0.219
71	J060709.47+390944.1	TYC 2925-320-1	06 07 09.47	+39 09 44.07	B7 III HgMn	247	9.6155	0.0006	1.1503	0.0708	−0.166	0.006	0.452	−0.532	0.134
72	J060712.43+243850.5	Gaia DR2 3423513793078031104	06 07 12.44	+24 38 48.86	B8 III–IV HgMn	442	10.6328	0.0003	1.0120	0.0429	−0.070	0.005	0.568	−0.091	0.092
73	J060732.64+215421.7	Gaia DR2 3375529467628181632	06 07 32.65	+21 54 21.76	B8 V (HgMn)	113	12.8900	0.0013	0.4509	0.4775	−0.207	0.409	1.260	−0.100	2.405
74	J060738.70+210326.1	Gaia DR2 3375294676288116320	06 07 38.70	+21 03 26.21	B8 IV–V HgMn	109	13.3276	0.0004	0.5674	0.0311	−0.392	0.466	1.641	+0.456	0.810
75	J060937.73+235218.0	HD 252428	06 09 37.73	+23 52 18.03	B8 III–IV HgMn	559	10.0629	0.0008	1.1282	0.0528	−0.106	0.005	0.582	−0.257	0.102
76	J061137.11+254307.8	TYC 1881-804-1	06 11 37.10	+25 43 07.87	B8 IV–V HgMn	231	11.9100	0.0003	0.5742	0.0642	−0.034	0.011	0.687	+0.018	0.243
77	J061144.23+245921.9	Gaia DR2 3426691381682039040	06 11 44.24	+24 59 21.95	B8 IV (HgMn)	108	13.3828	0.0004	0.2225	0.0322	−0.121	0.032	1.095	−0.976	0.319
78	J061237.92+331656.7	Gaia DR2 3452046261553987072	06 12 37.93	+33 16 56.72	B8 III–IV HgMn	107	13.1882	0.0003	0.4392	0.0257	+0.217	0.003	0.851	−0.550	0.127
79	J061436.72+252945.2	Gaia DR2 3426820038671293344	06 14 36.73	+25 29 45.30	B9 IV–V HgMn	170	12.3439	0.0003	0.7204	0.0560	+0.012	0.009	0.928	+0.704	0.169
80	J062219.81+224023.5	HD 255857	06 22 19.82	+22 40 23.54	B8 IV–V HgMn	428	10.6444	0.0006	1.1178	0.0636	−0.079	0.010	0.434	−0.453	0.125
81	J062425.14+190413.7	Gaia DR2 3373237049504772880	06 24 25.16	+19 04 13.74	B8 IV–V HgMn	118	14.6247	0.0005	0.2290	0.0336	+0.005	0.038	0.883	+0.541	0.325
82	J062503.02+033237.3 [d]	HD 256951	06 25 03.02	+03 32 37.33	B7 IV HgMn	345	10.5086	0.0005	1.0687	0.0847	−0.089	0.005	1.010	−0.357	0.172
83	J062524.46+224236.2	TYC 1879-333-1	06 25 24.47	+22 42 36.25	B9.5 IV HgMn	170	12.4303	0.0003	0.5753	0.0497	−0.249	0.055	1.025	+0.205	0.211
84	J062719.70+095803.7	Gaia DR2 3332748186769263776	06 27 19.71	+09 58 03.76	B9 III–IV (HgMn)	113	14.0369	0.0004	0.2443	0.0291	−0.049	0.023	1.218	−0.242	0.261
85	J063246.02+030319.1	TYC 150-604-1	06 32 46.03	+03 03 19.13	B8 IV HgMn	180	11.6210	0.0003	0.7336	0.0666	−0.749	0.078	1.985	−1.037	0.238
86	J063253.86+034220.3	HD 46338	06 32 53.87	+03 42 20.34	B8 V (HgMn)	188	9.6598	0.0005	1.4824	0.0465	−0.204	0.004	0.346	−0.169	0.068
87	J063735.23+210443.6	HD 260690	06 37 35.31	+21 04 43.76	B9 III–IV HgMn	565	10.5966	0.0006	1.7065	0.0866	−0.189	0.008	0.295	−0.453	0.266
88	J063821.84+110846.7	HD 261050	06 38 21.85	+11 08 46.76	B8 III HgMn	136	10.7161	0.0004	1.0286	0.0485	−0.024	0.003	1.550	−0.772	0.102
89	J063910.31+522527.3	HD 46980	06 39 10.32	+52 25 30.14	B8 IV HgMn	572	9.8145	0.0005	1.2655	0.0726	−0.119	0.004	0.155	+0.171	0.125
90	J063950.80+345537.7 [a]	TYC 2443-805-1	06 39 50.80	+34 55 37.79	B7 III–IV HgMn	188	10.1067	0.0007	0.9902	0.0443	−0.082	0.003	0.344	−0.259	0.097
91	J064224.70+130935.7	Gaia DR2 3352682021366285568	06 42 24.70	+13 09 35.66	B8 IV HgMn	162	14.2209	0.0004	0.2732	0.0459	−0.035	0.092	0.708	+0.695	0.399
92	J064424.23+280442.5	TYC 1901-773-1	06 44 24.23	+28 04 42.49	B8 IV HgMn	83	12.7250	0.0005	0.8249	0.0563	−0.141	0.007	0.160	+2.147	0.148
93	J064459.62+202512.7	TYC 1338-533-1	06 44 59.63	+20 25 12.72	B9 IV–V (HgMn)	260	12.1338	0.0005	0.4987	0.0898	−0.059	0.006	0.318	+0.305	0.391

Table A.1. continued.

(1) No.	(2) ID_LAMOST	(3) ID_alt	(4) RA(J2000)	(5) Dec(J2000)	(6) SpT_final	(7) $S/N g$	(8) G mag	(9) e_G mag	(10) pi (mas)	(11) e_pi	(12) $(BP-RP)_0$	(13) $e\_(BP-RP)_0$	(14) A_G	(15) M_{G0}	(16) e_M_{G0}
94	J064509.27+285032.7	HD 262952	06 45 09.27	+28 50 32.71	B6 III (HgMn)	132	11.1320	0.0009	0.5622	0.0550	−0.178	0.006	0.250	−0.368	0.212
95	J064604.00−024628.2	TYC 152-650-1	06 46 04.00	+02 46 28.27	B8 IV HgMn	181	11.7663	0.0003	0.7475	0.0444	−0.047	0.015	0.383	−0.752	0.131
96	J064642.68+074808.3	Gaia DR2 3133992491496045184	06 46 42.69	+07 48 08.34	B9 III HgMn	106	12.4021	0.0003	0.7542	0.0428	−0.122	0.008	0.638	+1.151	0.124
97	J065006.33−023041.0	Gaia DR2 3126488805672228352	06 50 06.34	+02 30 41.09	B8 IV (HgMn:)	128	13.0658	0.0006	0.4873	0.0354	−0.012	0.020	0.710	−0.794	0.161
98	J065011.54+014917.3 [a]	TYC 148-118-1	06 50 11.54	+01 49 17.43	B8 IV HgMn	183	11.8240	0.0003	0.6449	0.0384	−0.046	0.004	0.457	+0.414	0.129
99	J065237.92+323912.9	TYC 2440-341-1	06 52 37.92	+32 39 13.01	B8 IV (HgMn)	176	12.1561	0.0004	0.5164	0.0541	−0.195	0.004	0.303	+0.418	0.227
100	J065253.84−005714.3	TYC 4801-1648-1	06 52 53.84	−00 57 14.38	B8 V HgMn	196	11.4605	0.0003	0.6814	0.0552	−0.104	0.011	0.479	−0.149	0.177
101	J065545.39−093941.0	HD 266502	06 55 45.30	+09 39 41.06	B8 III–IV HgMn	236	10.6756	0.0006	0.8030	0.0507	−0.096	0.008	0.312	−0.113	0.138
102	J065942.88−039951.0	HD 289522	06 59 42.89	+00 39 51.03	B9.5 IV–V (HgMn)	332	11.2633	0.0006	0.9924	0.0442	−0.125	0.005	0.384	+0.863	0.097
103	J071933.80+145655.7	HD 56914	07 19 33.80	+14 56 55.76	B8 IV HgMn	348	9.0445	0.0006	1.3497	0.0874	−0.084	0.004	0.099	−0.404	0.141
104	J072016.47+141320.6 [a]	HD 57109	07 20 16.48	+14 13 20.58	B8 IV HgMn	289	9.0677	0.0004	1.4537	0.0540	−0.129	0.003	0.170	−0.290	0.081
105	J072147.31+245451.4	HD 57338	07 21 47.32	+24 54 51.50	B9 IV HgMn	593	9.5273	0.0013	0.9135	0.0804	−0.122	0.021	0.156	−0.825	0.191
106	J072836.11+095219.2	TYC 768-1132-1	07 28 36.11	+09 52 19.20	B8 IV HgMn	144	11.8213	0.0005	0.6217	0.0553	−0.165	0.008	0.099	+0.690	0.193
107	J074457.09+541600.8	TYC 3782-390-1	07 44 57.10	+54 16 00.82	B8 III–IV HgMn	247	10.9709	0.0007	0.7474	0.0709	−0.174	0.004	0.181	−0.158	0.206
108	J091838.94+195023.7	Gaia DR2 2635840844129715712	09 18 38.95	+19 50 23.76	B9 IV–V HgMn	130	13.1622	0.0003	0.3847	0.0551	−0.141	0.003	0.086	+1.002	0.311
109	J112400.77+540532.1	TYC 3825-801-1	11 24 00.21	+54 05 30.76	B8 IV (HgMn:)	107	11.7136	0.0005	2.8385	0.2800	−0.120	0.004	0.073	+3.906	0.214
110	J130109.88−031648.1	Gaia DR2 2368509458647559040	13 01 09.88	−03 16 48.15	B8 IV (HgMn)	108	13.0938	0.0005	0.5376	0.0748	−0.203	0.004	0.093	+1.653	0.302
111	J133147.11−023941.1	Gaia DR2 3637524870906723328	13 31 47.14	−02 39 41.98	B8 IV HgMn	195	13.4212	0.0005	0.4261	0.0398	−0.169	0.004	0.105	+1.464	0.203
112	J154534.12−160842.8	Gaia DR2 2119614529955569792	15 45 34.13	+16 08 42.80	B8 IV HgMn	188	12.7487	0.0003	0.4955	0.0734	−0.202	0.004	0.166	+1.058	0.321
113	J184142.65+482514.8	TYC 3551-659-1	18 41 42.64	+48 25 13.73	B8 IV HgMn	137	11.2487	0.0007	1.3830	0.0451	−0.198	0.005	0.174	+1.778	0.071
114	J192837.06+520029.0	TYC 3555-1845-1	19 28 37.06	+52 00 29.17	B8 IV (HgMn)	133	12.3400	0.0003	0.2319	0.0202	−0.058	0.003	0.269	−1.102	0.189
115	J194139.54+403833.9 [a]	HD 186254	19 41 39.28	+40 38 33.72	B8 IV HgMn	184	8.5859	0.0005	1.6616	0.0662	−0.124	0.008	0.209	−0.520	0.088
116	J195021.63+411958.5	Gaia DR2 2207687363404644800	19 50 21.63	+41 19 58.60	B9 IV HgMn	147	13.2381	0.0003	0.3797	0.0189	−0.057	0.013	0.931	+0.204	0.110
117	J195652.72+270157.7	Gaia DR2 2027500408007197824	19 56 52.72	+27 01 57.81	B8 V HgMn	184	12.1590	0.0001	0.8913	0.0277	+0.004	0.003	1.186	−0.723	0.068
118	J202548.00+363352.4	Gaia DR2 2057692374515650816	20 25 48.01	+36 33 52.47	B7 IV–V HgMn	140	12.4641	0.0002	0.7678	0.0261	−0.405	0.051	2.046	−0.156	0.114
119	J205110.47+355929.8	TYC 2700-379-1	20 51 10.47	+35 59 29.81	B7 IV (Hg)Mn	253	11.3640	0.0009	0.7526	0.0425	−0.190	0.008	0.566	−0.180	0.123
120	J213215.68+425837.2	Gaia DR2 1967805344746109696	21 32 15.69	+42 58 37.34	B8 IV–V (HgMn)	119	12.8857	0.0003	0.5965	0.0291	+0.105	0.002	0.967	−0.797	0.106
121	J213851.08+164506.8	Gaia DR2 1773423160802357376	21 38 51.10	+16 45 07.28	B6 III HgMn	230	13.4933	0.0005	0.1242	0.0382	−0.191	0.004	0.363	−1.399	0.667
122	J230239.47+555203.1	TYC 3989-742-1	23 02 39.47	+55 52 03.14	B9 IV–V HgMn	193	11.8371	0.0003	0.7309	0.0304	+0.021	0.004	0.443	+0.713	0.090
123	J231115.48+543738.0	TYC 4002-1726-1	23 11 15.49	+54 37 38.01	B8 IV HgMn	174	10.9405	0.0007	1.0549	0.0453	−0.142	0.006	0.576	+0.481	0.094
124	J231124.89+570726.6	TYC 4006-596-1	23 11 24.89	+57 07 26.63	B8 IV–V HgMn	156	11.3446	0.0005	0.9658	0.0319	−0.005	0.002	0.984	+0.285	0.072
125	J232346.41+551605.3	TYC 4003-471-1	23 23 46.41	+55 16 05.32	B8 IV–V HgMn	195	11.8367	0.0003	0.5395	0.0330	−0.125	0.005	0.446	+0.051	0.133

Table A.2. Upper limits of variability for the stars identified as non-variable in the accuracy limits of the employed data sources.

(1) No.	(2) ID_LAMOST	(3) UL_{SW}	(4) UL_{AS}	(5) UL_{AS3}	(6) UL_{TE}	(1) No.	(2) ID_LAMOST	(3) UL_{SW}	(4) UL_{AS}	(5) UL_{AS3}	(6) UL_{TE}
1	J000118.65+464355.0	4.7				61	J055457.96+092830.5		3.8	10.3	0.5
2	J002635.94+562206.5		5.7			62	J055505.90+212949.6	4.5	4.1		
3	J020922.72+533908.6	5.7	2.8			63	J055744.95+255028.1	9.7			
4	J030852.02+553734.3	2.4	3.2			64	J055811.62+303219.5	25.1	3.5		
5	J031312.82+493559.8	4.0	3.5			65	J055854.37+292654.8	3.0	3.0		
6	J031943.49+561329.7	2.7	7.5			66	J060122.46+301948.7	4.7	4.0		
7	J032252.69+582806.7	10.0	7.6			67	J060238.73+295105.4	2.5	3.2		
8	J033700.61+571139.0	3.0	3.2			68	J060405.77+290624.1	3.4	6.2		
9	J033939.69+473758.3	12.1	2.0			69	J060605.43+290405.2	2.7	3.3		
10	J034903.76+454037.3	4.9				70	J060619.07+345118.1	2.8	4.4		
11	J035332.73+523248.9	19.2	3.4			71	J060709.47+390944.1	2.8			
12	J035333.90+524118.7	8.4	3.8			72	J060712.43+243850.5	2.5	5.4		
13	J035805.60+452213.6	4.6	2.8			73	J060732.64+215421.7	44.2	4.8		
14	J040155.24+514923.5	3.6	5.0			74	J060738.70+210326.1	4.5	7.2		
15	J040437.83+460141.5	3.5	2.6			77	J061144.23+245921.9	9.6	10.8		
16	J041102.63+513103.7	4.7	5.9			78	J061237.92+331656.7	2.5	5.5		
17	J041115.00+360322.2	2.3	7.0			79	J061436.72+252945.2	3.4	6.2		
18	J041446.58+454448.3	8.0	4.0			80	J062219.81+224023.5	5.7	3.2		
19	J041533.86+493944.1	6.7				81	J062425.14+190413.7	6.1			
20	J041632.64+424344.2	2.7	5.0			82	J062503.02+033237.3		5.0	10.0	0.4
21	J042204.78+482811.3	5.7	6.8			83	J062524.46+224236.2		4.9		
22	J042726.80+525506.2					84	J062719.70+095803.7				0.7
23	J042829.12+511637.5	2.1				85	J063246.02+030319.1		9.9	11.0	0.5
24	J042908.75+530654.3	2.1	3.5			89	J063910.31+522527.3	4.8			
25	J043338.55+523755.1	6.5				90	J063950.80+345537.7	3.2			
26	J043743.94+414133.8	5.0	5.7			91	J064224.70+130935.7			20.2	
27	J044429.05+554643.2	15.4	11.0			92	J064424.23+280442.5	1.8	5.4		
28	J044732.75+482124.5	5.8	5.3			93	J064459.62+202512.7		4.6		
29	J045516.12+581945.5	6.5	5.8			94	J064509.27+285032.7	2.0	3.2		
31	J050740.17+380705.1	2.0	3.0			95	J064604.00+024628.2		4.6	11.8	0.4
32	J050810.73+453321.8	2.8	2.4			96	J064642.68+074808.3		6.9	20.0	0.4
33	J051309.48+551742.2	2.5	3.7			97	J065006.33+023041.0		7.0		0.5
34	J051503.39+323903.2	20.0	10.9			98	J065011.54+014917.3		3.0	11.1	0.4
35	J051625.06+563321.2	3.4	4.8			99	J065237.92+323912.9	3.6	4.5		
36	J051813.77+452059.7	1.3	3.0			100	J065253.84−005714.3		6.2	10.5	0.4
37	J052056.26+085723.5		3.5	4.2		101	J065545.39+093941.0		7.1	10.8	0.4
38	J052119.19+370619.9	2.6	5.6			102	J065942.88+003951.0		6.0	10.0	
39	J052308.77+323128.3	1.7	4.5			104	J072016.47+141320.6			7.0	0.4
40	J052436.09+321553.5	5.8	5.1			105	J072147.31+245451.4	2.8			
41	J052606.26+321808.6	3.8	4.5			106	J072836.11+095219.2		5.7	12.3	0.4
42	J052649.33+431004.9	3.2	5.7			107	J074457.09+541600.8	11.6	6.0		
43	J052746.31+314215.9	1.5	4.0			108	J091838.94+195023.7		9.2		
44	J052808.91+315213.3	1.8				109	J112400.77+540532.1		6.0		
45	J053028.44+060100.9		4.5	19.8	0.5	110	J130109.88−031648.1		1.8		
46	J053419.30+302407.7	5.2				111	J133147.11−023941.1		7.3		
47	J053513.37+192705.9		4.2	25.1		112	J154534.12+160842.8		5.6		
48	J053642.85+240205.8	2.4	6.1			113	J184142.65+482514.8	8.4	33.0		0.4
49	J053819.93+392350.0	5.4	2.7			114	J192837.06+520029.0	5.4	5.9		0.4
50	J053836.11+340929.7	2.3	3.3			115	J194139.54+403833.9				0.4
51	J054033.05+331124.6	3.2				117	J195652.72+270157.7		8.2		0.5
52	J054052.69+215844.5	2.8				118	J202548.00+363352.4	4.3	4.9		0.5
53	J054619.47+260416.7	2.3				119	J205110.47+355929.8		9.3		0.4
54	J054927.98+302256.1	2.6	2.6			120	J213215.68+425837.2	4.0	11.0		0.5
55	J055005.52+152159.5		6.5	14.0	0.3	121	J213851.08+164506.8		10.0		
56	J055030.45+244900.6	3.1	4.7			122	J230239.47+555203.1	8.1	5.4		0.4
57	J055116.00+420914.5	5.6	10.3			123	J231115.48+543738.0	6.2	8.4		
58	J055213.34+325807.7	2.8	8.3			124	J231124.89+570726.6	13.3	4.7		
59	J055309.48+265424.2	2.3	3.1			125	J232346.41+551605.3	5.8	17.3		
60	J055400.30+290112.2	3.3	2.3								

Notes. The columns denote: (1) Internal identification number. (2) LAMOST identifier. (3) Upper limit of variability as derived from SWASP data. (4) Upper limit of variability as derived from ASAS-SN data. (5) Upper limit of variability as derived from ASAS-3 data. (6) Upper limit of variability as derived from TESS data. All values denote semiamplitudes given in millimagnitudes.